On convex numerical schemes for inelastic contacts with friction

Hélène Bloch, Aline Lefebvre-Lepot

On convex numerical schemes for inelastic contacts with friction*

Hélène Bloch† Aline Lefebvre-Lepot†

March 1, 2024

Abstract

This paper reviews the different existing Contact Dynamics schemes for the simulation of granular media, for which the discrete incremental problem is based on the resolution of convex problems. This type of discretization has the great advantage of allowing the use of standard convex optimization algorithms. In the case of frictional contacts, we consider schemes based on a convex relaxation of the constraint as well as a fixed point scheme. The model and the computations leading to the discrete problems are detailed in the case of convex, regular but not necessarily spherical particles. We prove, using basic tools of convex analysis, that the discrete optimization problem can be seen as a minimization problem of a global discrete energy for the system, in which the velocity to be considered is an average of the pre- and post-impact velocities. A numerical study on an academic test case is conducted, illustrating for the first time the convergence with order 1 in the time step of the different schemes. We also discuss the influence of the convex relaxation of the constraint on the behavior of the system. We show in particular that, although it induces numerical dilatation, it does not significantly modify the macrosopic behavior of a column collapse en 2d. The numerical tests are performed using the code SCoPI.

Introduction

We consider granular materials composed of solid particles of macroscopic size in the sense that they are large enough not to be subject to Brownian forces. They can interact through a wide variety of inter-particle forces and are subject to dissipative contacts that may involve friction. Such systems are omnipresent in our daily lives (sugar, rice, pasta in the kitchen...), in nature (piles of sand, dunes, sandy coasts, rock avalanches...), in industry (grain silos, storage of medicines...). These systems made of macroscopic particles can also be immersed in a viscous fluid. They are then called suspensions. Suspensions are present in various fields, both industrial (waste treatment, concrete, transport of pastes or granules...), natural (silting, coastal dynamics, landslides, dispersion of pollutants...) or sanitary (wastewater treatment...).

Although they are present in everyday life, the flow properties of these systems are still partly not understood. It is now well established that a better understanding of their behaviour requires numerical simulations at the particle scale. It is then necessary to develop models and efficient algorithms in order to take into account the contact phenomena, with or without friction, for systems involving large numbers of particles. A great amount of work has been performed on the subject and multiple modeling strategies and numerical schemes have been developed to solve this problem. The so-called Discrete Element Methods (DEM) include approaches based on particle-scale models and simulations, as opposed to macroscopic continuous models. Among these discrete methods, two classes of models can be distinguished.

The first, identified as a "soft" method, is the so-called Molecular Dynamics approach (MD). It goes back to the work of Cundall and Strack [12]. The contact between the particles is penalized by an explicit contact force, modeled by Hertz-like contact laws between slightly deformable particles. The fundamental principle of dynamics including the corresponding forces is then solved. A description of this method can be found in [25] and a recent review of the large choice of models for the forces is given in [11]. If MD provides good results in many situations, it leads to the resolution of stiff ODEs (the contact forces become very large as the grains approach each other). Moreover, the models involve a large number of parameters and the method is therefore subject to a delicate calibration step.

A second class of methods, identified as "hard" methods, is the so-called Contact Dynamics approach (CD), developed by Moreau and Jean in the 1990s. The model is limited to the main features of the

*The authors warmly thank Sylvain Faure and Loïc Gouarin, for their key contribution to the development of the code SCoPI, which allowed to perform the numerical tests presented in this article. This work was supported by the French National Research Agency (ANR) through Grant ANR18-CE46-0005 (project RheoSuNN)

†CMAP, CNRS, Ecole Polytechnique, Institut Polytechnique de Paris, 91128 Palaiseau, France (aline.lefebvre@polytechnique.edu).

contact, such as the non-overlapping of the grains, without further refinement. We refer to the seminal papers [31, 19, 32, 18] for a detailed description of the so-called Non-Smooth Contact Dynamics method (NSCD). The corresponding model fall into the framework of non-smooth convex analysis. The contact forces are implicit, belong to the friction Coulomb cone and are deduced from the Lagrange multipliers associated with the non-interpenetration constraints. This solves the difficulty due to the stiffness of the forces and makes it possible to obtain stable algorithms, supporting large time-steps. After time discretization, the discrete incremental problem to be solved at each time-step is a non-convex Linear Complementarity Problem (LCP), which is known to be difficult to solve numerically. A review of the main existing algorithms to tackle this problem can be found in [1]. One can cite for example algorithms based on a faceted discretization of Coulomb cone, on variational inequalities formulations or on non-smooth equations, and using projection/splitting methods, Gauss-Seidel like relaxations or generalized Newton methods. Unfortunately, unless in the case of a faceted cone, no general convergence results for the corresponding iterative methods are available.

Later, some authors proposed CD schemes for which the incremental problem comes down to solving convex problems. The main advantage of these formulations is that there are many algorithms available to solve the discrete problem and for which there exists convergence results. A convex formulation is for example proposed in [43, 7], where the authors use a convex relaxation of the non-overlapping constraint. The discrete problem then comes down to solving a Conic Complementarity Problem (CCP), which can be achieved using Projected Jacobi or Gauss-Seidel Jacobi methods. The CCP problem can also be viewed as a quadratic optimization problem with second order conic constraints. This allows the use of several existing optimization solvers. For example, it can be solved by accelerated projected gradient descent methods [28, 13], various spectral and Krylov subspace methods [16] or interior point methods [37, 20, 3, 10]. To avoid the convex relaxation of the problem, the authors in [2] propose to iterate a fixed point functional to solve the original LCP problem. Each iteration of the fixed point reduces to solving a CCP problem similar to the one obtained by convexifying the constraint.

Beyond the difficulty of numerically solving the incremental problem, the question of the convergence of the different schemes when the time-step vanishes is a also difficult question for which few results are available. Some convergence results of numerical schemes for granular materials were obtained in the case of a single contact in [36, 27, 30] and for multiple contacts without friction in [9]. For frictional systems, one can also cite [40, 4] proving the convergence of numerical schemes for the faceted Coulomb cone.

In this paper, we describe and investigate the behavior of these different convex approaches for granular media. The document is intended to be self-contained, so the model and computations leading to the discrete problems are detailed. Section 1 is dedicated to the frictionless case. In Section 2, we consider the two schemes leading to convex problems in the frictional case: the one resulting from a convex relaxation of the non-overlapping constraint, and its coupling with a fixed point method. These methods are based on global minimization problems for the unknown velocity. In both sections, we compute the corresponding optimality conditions using basic tools of convex analysis. As expected, it leads to a discretization of the fundamental principle of dynamics, for which discrete Coulomb laws are verified locally. We prove that the discrete optimization problem can also be seen as a global discrete energy minimization problem for the system, in which the velocity to be considered is an average of the pre- and post-impact velocities. This echoes the definition of energy proposed by Frémond in [15] for the undiscretized model. Section 3 is devoted to numerical tests for the non-frictional scheme and the two convex schemes for friction. After discussing the algorithms that can be used to solve the incremental problem, we perform a numerical study of the convergence for the different schemes when the time-step vanishes. The speed of convergence of the schemes had not been theoretically nor numerically studied until now. We observe that all the schemes considered converge with order one in the time-step. The convergence studies are conducted on an academic test case (a sphere falling on an inclined plane), for which an exact solution is available. Finally, we present some tests in the multi-particle case. We compare the macroscopic behavior of the solutions computed using constraint convexification to that of the solutions to the original non-convex problem, obtained using the fixed point algorithm. Finally, a test case involving ellipsoidal particles is reported. The notion of subdifferential is the basic tool of convex analysis that will be used in the frictional case, as an extention of the notion of derivative for convex functions. In order to be self-contained, appendix A allows the reader to become familiar with this notion if needed. Moreover, following the same objective, the computation of the explicit solution for the sphere falling on an inclined plane is given in appendix B.

1 Convex schemes for frictionless contacts

In this first section, we focus on the inelastic frictionless contact problem. The corresponding model is presented together with a convex scheme that can be used to approximate the solutions. The scheme is based

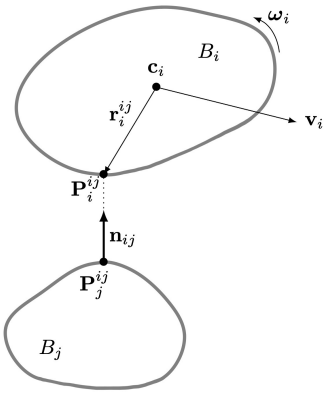

Figure 1: Notations

on a constrained minimization problem for the generalized velocity vector. It is a straightforward extension to non-spherical particles of the scheme proposed [27]. We show that the corresponding dual problem can be seen as a discrete global energy minimization problem.

1.1 Notations

1.1.1 Particles description

Let us consider a mechanical system in $\mathbb{R}^3$, composed of N convex rigid bodies, with regular boundaries. The configuration of the i-th body B_i is given by $(\mathbf{c}_i, \boldsymbol{\sigma}_i)$, where $\mathbf{c}_i \in \mathbb{R}^3$ is the position of its center of mass and $\boldsymbol{\sigma}_i \in \mathbb{R}^p$ its orientation. The orientation can be represented by Euler angles – $p = 3$ – or normalized quaternions – $p = 4$ – for example. We denote by

$$\mathbf{c} = (\mathbf{c}_1, \boldsymbol{\sigma}_1, \dots, \mathbf{c}_N, \boldsymbol{\sigma}_N) \in \mathbb{R}^{(3+p)N}$$

the generalized position vector.

The instantaneous velocity and instantaneous rotation vector for particle i are denoted by $\mathbf{v}_i \in \mathbb{R}^3$ and $\boldsymbol{\omega}_i \in \mathbb{R}^3$ respectively. In order to deal with constant moments of inertia, it is convenient to use local moving frames linked to each solid. We denote by $(\mathbf{e}_1, \mathbf{e}_2, \mathbf{e}_3)$ the fixed frame of reference and $(\mathbf{e}'_{1,i}, \mathbf{e}'_{2,i}, \mathbf{e}'_{3,i})$ the moving frame linked to particle i:

$$\mathbf{e}_k = R_i \mathbf{e}'_{k,i}\,,\ k = 1 \dots 3\,,\ i = 1 \dots N,$$

where R_i is the rotation matrix giving the orientation of particle i. The instantaneous rotation vector of particle i in the moving frame linked to particle i is then given by

$$\boldsymbol{\omega}'_i = R_i \boldsymbol{\omega}_i$$

and we define the corresponding generalized velocity vector as

$$\mathbf{u} = (\mathbf{v}_1, \boldsymbol{\omega}'_1, \dots, \mathbf{v}_N, \boldsymbol{\omega}'_N) \in \mathbb{R}^{6N}.$$

We finally define the $6N \times 6N$ generalized mass matrix as

$$\mathbf{M} = \mathrm{diag}\,(m_1, m_1, m_1, J_{1,1}, J_{2,1}, J_{3,1}, m_2, \dots, J_{1,N}, J_{2,N}, J_{3,N})\,,$$

where m_i and $J_{k,i}$, $k = 1 \dots 3$ are the mass and (constant) moments of inertia of particle i, given in the moving frame linked to the particle.

1.1.2 Contacts description

We denote by I_c the set of all possible pairs of contacts: $I_c = \{(i,j)\ 1 \le i < j \le N\}$. Note that the pair of grains i and j is represented only once in I_c through the couple (i,j) if $i < j$ and (j,i) if $j < i$.

For any two grains i and j with $(i,j) \in I_c$, we denote by $\mathbf{P}_i^{ij}$ and $\mathbf{P}_j^{ij}$ the points which realize the distance between the grains (with $\mathbf{P}_i^{ij} = \mathbf{P}_j^{ij}$ if the two grains are in contact), see Figure 1. We define the associated position vectors $\mathbf{r}_i^{ij} = \mathbf{P}_i^{ij} - \mathbf{c}_i$, $\mathbf{r}_j^{ij} = \mathbf{P}_j^{ij} - \mathbf{c}_j$.

The normal direction to the surfaces of the particles at points $\mathbf{P}_i^{ij}$ and $\mathbf{P}_j^{ij}$, which is shared by the two particles. We introduce the unit vector $\mathbf{n}_{ij}$, defined as the outer normal vector to particle j at point $\mathbf{P}_j^{ij}$. The signed distance between particles i and j is then defined by :

$$D_{ij}(\mathbf{c}) = (\mathbf{P}_i^{ij} - \mathbf{P}_j^{ij}) \cdot \mathbf{n}_{ij},$$

so that the non-overlapping condition writes $D_{ij} \geq 0$.

Finally, we define the projections on the normal direction and on Π_{ij}, the tangent plane to the surfaces, which is orthogonal to $\mathbf{n}_{ij}$: for $\mathbf{v} \in \mathbb{R}^3$

$$\begin{aligned} N_{ij}\mathbf{v} &= \mathbf{v} \cdot \mathbf{n}_{ij} \in \mathbb{R}, \\ T_{ij}\mathbf{v} &= \mathbf{v} - (\mathbf{v} \cdot \mathbf{n}_{ij})\mathbf{n}_{ij} \in \mathbb{R}^3, \end{aligned}$$

so that we can decompose any vector $\mathbf{v} \in \mathbb{R}^3$ in a local normal and tangential part:

$$\mathbf{v} = v_n^{ij}\mathbf{n}_{ij} + \mathbf{v}_T^{ij} \text{ where } v_n^{ij} = N_{ij}\mathbf{v}\,,\ \mathbf{v}_T^{ij} = T_{ij}\mathbf{v}.$$

In what follows, the subscripts n (resp. T), will designate the quantities corresponding to the normal coordinates (resp. tangential components) of vectors.

1.1.3 From particles to contacts

We define A_{ij} as the linear operator which maps the generalized velocity field $\mathbf{u} \in \mathbb{R}^{6N}$ to the relative velocity between the points $\mathbf{P}_i^{ij}$ and $\mathbf{P}_j^{ij}$ at which the distance between spheres i and j is attained , i.e.

$$\begin{aligned} A_{ij}\mathbf{u} &= (\mathbf{v}_i + \boldsymbol{\omega}_i \wedge \mathbf{r}_i^{ij}) - (\mathbf{v}_j + \boldsymbol{\omega}_j \wedge \mathbf{r}_j^{ij}) \\ &= (\mathbf{v}_i - \mathbf{r}_i^{ij} \wedge R_i\boldsymbol{\omega}_i') - (\mathbf{v}_j - \mathbf{r}_j^{ij} \wedge R_j\boldsymbol{\omega}_j') \in \mathbb{R}^3. \end{aligned}$$

Straightforward computations show that, for any generalized velocity $\mathbf{u} \in \mathbb{R}^{6N}$ and any vector $\mathbf{f} \in \mathbb{R}^3$, we have $A_{ij}\mathbf{u} \cdot \mathbf{f} = \mathbf{u} \cdot A_{ij}^T\mathbf{f}$ with

$$A_{ij}^T\mathbf{f} = (\mathbf{0}, \ldots, \mathbf{0}, \underbrace{\mathbf{f}, R_i^T(\mathbf{r}_i^{ij} \wedge \mathbf{f})}_{\text{position } i}, \mathbf{0}, \ldots, \mathbf{0}, \underbrace{-\mathbf{f}, -R_j^T(\mathbf{r}_j^{ij} \wedge \mathbf{f})}_{\text{position } j}, \mathbf{0}, \ldots, \mathbf{0}) \in \mathbb{R}^{6N},$$

so that A_{ij}^T maps a vector $\mathbf{f} \in \mathbb{R}^3$ to the generalized force/moment vector corresponding to the force $\mathbf{f}$ exerted on particle i at point $\mathbf{P}_i^{ij}$ and the opposite force $-\mathbf{f}$ exerted on particle j at point $\mathbf{P}_j^{ij}$ (the moments being in the local reference frames linked to the particles) .

The real $N_{ij}A_{ij}\mathbf{u}$ and the vector $T_{ij}A_{ij}\mathbf{u}$ represent the normal and tangential relative velocities respectively. As a consequence, when two spheres are in contact with no relative normal motion, i.e. $N_{ij}A_{ij}\mathbf{u} = 0$, then $T_{ij}A_{ij}\mathbf{u} = 0$ expresses a rolling motion with no slip, while $T_{ij}A_{ij}\mathbf{u} \neq 0$ corresponds to a sliding motion.

1.2 Inelastic contact modeling

The specificity of the Contact Dynamics models lies in the fact that they explicitly express that two rigid bodies cannot interpenetrate. This means that, for all $\alpha = (i, j) \in I_c$, the distance D_α must remain non negative. Then, the set of *admissible configurations* is:

$$\mathcal{Q} = \left\{ \mathbf{c} \in \mathbb{R}^{(3+p)N} \quad \text{s.t.} \quad D_\alpha(\mathbf{c}) \geq 0\,,\ \forall \alpha \in I_c \right\}.$$

Since there is no friction, for all $\alpha = (i, j)$ in I_c, the corresponding contact force $\mathbf{f}^\alpha$ (also denoted $\mathbf{f}^{ij}$) exerted on particle i at point $\mathbf{P}_i^{ij}$ is a repulsive force, collinear to $\mathbf{n}_\alpha$:

$$\mathbf{f}^\alpha = f_n^\alpha\, \mathbf{n}_\alpha \quad \text{where} \quad f_n^\alpha \geq 0.$$

The contact force exerted on particle j is $\mathbf{f}^{ji} = -\mathbf{f}^{ij} = -\mathbf{f}^\alpha$. Moreover, the contact force must vanish as soon as the contact is broken. This can be expressed by the equality $D_\alpha f_n^\alpha = 0$ which implies that $\mathbf{f}^\alpha$ cannot be active (i.e. it has to vanish) as long as the distance is not zero. These conditions are known as the *Signorini conditions*:

$$D_\alpha(\mathbf{c}) \geq 0\,,\ f_n^\alpha \geq 0\,,\ D_\alpha(\mathbf{c})\, f_n^\alpha = 0\,,\ \forall \alpha \in I_c. \tag{1}$$

We will see later that the force f_n^α can be seen as the Lagrange multiplier associated to the constraint $D_\alpha \geq 0$. The last equality in Signorini conditions is the corresponding complementarity condition.

When two rigid bodies come into contact, expressing the Signorini condition is not sufficient to determine the motion. Indeed, if the reaction f_n^α must be positive, no information is given on its value. The model lacks an impact law, relating the normal impact velocity before contact to the velocity after contact. Using the fact that

$$\frac{dD_\alpha(\mathbf{c})}{dt} = dD_\alpha(\mathbf{c})\frac{d\mathbf{c}}{dt}$$

where $dD_\alpha(\mathbf{c})$ is the differential of D_α at $\mathbf{c}$, one can for example write the inelastic contact law as:

$$\mathbf{u}^+ = P_{\mathcal{C}_\mathbf{c}}\mathbf{u}^- \quad \text{with} \quad \mathcal{C}_\mathbf{c} = \left\{\mathbf{u} \in \mathbb{R}^{6N}, \quad \text{s.t.} \quad dD_\alpha(\mathbf{c})\mathbf{u} \geq 0 \text{ if } D_\alpha(\mathbf{c}) = 0\,,\ \forall \alpha \in I_c\right\}, \tag{2}$$

where $\mathbf{u}^+$ (resp. $\mathbf{u}^-$) is the right-sided (resp. left-sided) limit of function $t \mapsto \mathbf{u}(t)$ and P denotes the projection in $\mathbb{R}^{6N}$. The set $\mathcal{C}_\mathbf{c}$ is the so-called set of *admissible velocities*. It reflects the fact that, to avoid overlaps, the distance must increase as soon as it vanishes.

Let us note, at this point of the discussion, that the velocity of the particle is likely to be non-smooth. In particular, the post-collisional velocity $\mathbf{u}^+$ can be different from the pre-collisional velocity $\mathbf{u}^-$. This raises the question of the meaning to be given to the different equations stated. To deal with the discontinuous character of the velocity, the space to consider is the space of functions with bounded variations. This allows to define the velocities before and after contact time. In that case, the force f_n^α is an impulse at contact time and, since the distance is continuous, the Signorini conditions can be understood in the sense of distributions or even in the sense of measures.

We can now state the equations of dynamics, driven by the fundamental principle of dynamics. If $(\mathbf{f}_i^{ext}, \mathbf{t}_i^{ext}) \in (\mathbb{R}^3)^2$ are the external force and torque exerted on particle i, the fundamental principle of dynamics writes for particle i:

$$\begin{aligned}
m_i \frac{d\mathbf{v}_i}{dt} &= \mathbf{f}_i^{ext} + \sum_{j,j\neq i}(f_n^{ij}\mathbf{n}_{ij} + \mathbf{f}_T^{ij}) && \forall i = 1\dots N,\\
J_i \frac{d\boldsymbol{\omega}_i'}{dt} &= -\boldsymbol{\omega}_i' \wedge (J_i\boldsymbol{\omega}_i') + R_i^T\mathbf{t}_i^{ext} + R_i^T\left(\sum_{j,j\neq i}\mathbf{r}_i^{ij} \wedge (f_n^{ij}\mathbf{n}_{ij} + \mathbf{f}_T^{ij})\right) && \forall i = 1\dots N,
\end{aligned}$$

where the equation for the rotational velocity $\boldsymbol{\omega}_i'$ is written in the moving frame linked to particle i. Note that, in case of spherical particles, the moment matrix do not depend on the frame and is diagonal. In that case, the second equation can be written for $\boldsymbol{\omega}_i$ in the fixed frame, the wedge product is zero and the rotation matrix is replaced by the identity matrix.

To finish, we define the generalized force vector as $\mathbf{f}^{ext} = (\mathbf{f}_1^{ext}, R_1^T\mathbf{t}_1^{ext}, \dots, \mathbf{f}_N^{ext}, R_N^T\mathbf{t}_N^{ext}) \in \mathbb{R}^{6N}$, $\mathbf{k}(\mathbf{u}) = (0, -\boldsymbol{\omega}_1' \wedge (J_1\boldsymbol{\omega}_1'), \dots, 0, -\boldsymbol{\omega}_N' \wedge (J_N\boldsymbol{\omega}_N')) \in \mathbb{R}^{6N}$ and $\mathbf{F}(\mathbf{u}) = \mathbf{f}^{ext} + \mathbf{k}(\mathbf{u})$. The equations of motion writes, in the sense of distributions or measures:

$$\frac{d\mathbf{c}}{dt} = \mathcal{L}(\mathbf{u}), \tag{3}$$

$$\mathbf{M}\frac{d\mathbf{u}}{dt} = \mathbf{F}(\mathbf{u}) + \sum_{\alpha\in I_c} A_\alpha^T f_n^\alpha \mathbf{n}_\alpha, \tag{4}$$

$$D_\alpha(\mathbf{c}) \geq 0\,,\ f_n^\alpha \geq 0\,,\ D_\alpha(\mathbf{c})\, f_n^\alpha = 0\,,\ \forall \alpha \in I_c, \tag{5}$$

$$\mathbf{u}^+ = P_{\mathcal{C}_\mathbf{c}}\mathbf{u}^-, \tag{6}$$

$$\mathbf{c}(0) = \mathbf{c}_0, \quad \mathbf{u}(0) = \mathbf{u}_0, \tag{7}$$

where the initial conditions $(\mathbf{c}_0, \mathbf{u}_0)$ are given and the operator $\mathcal{L}$ in the first equation provides the evolution equation for $\mathbf{c}$ and depends on the chosen parametrization for the rotations.

1.3 Convex numerical schemes: an affine constraint

In this subsection we present a time-step scheme to approximate the solution to (3,7) by solutions of a discrete minimization problem under affine constraints as proposed in [27]. We show that this problem rewrites as a discrete energy minimization problem.

1.3.1 A discrete set of admissible velocities

We denote the time-step by Δt, by $\mathbf{c}^k$ the configuration of the particles at time $k\Delta t$ and by $\mathbf{u}^k \in \mathbb{R}^{6N}$ the generalized velocities at step k. The scheme is based on a Euler discretization to compute the position of the centers at time $k+1$:

$$\mathbf{c}_i^{k+1} = \mathbf{c}_i^k + \Delta t\, \mathbf{v}_i^{k+1}.$$

Similarly, the orientations $\boldsymbol{\sigma}_i^{k+1}$ are computed from $\boldsymbol{\sigma}_i^k$, $\mathbf{v}_i^{k+1}$ and $\boldsymbol{\omega}_i^{k+1}$. The corresponding scheme depends on the chosen representation of the orientation.

It now remains to describe how to compute $\mathbf{u}^{k+1}$. Denoting by $\mathbf{v}(\mathbf{P}_i^{ij}) = \mathbf{v}_i + \boldsymbol{\omega}_i \wedge \mathbf{r}_i^{ij} \in \mathbb{R}^3$ the velocity of point $\mathbf{P}_i^{ij}$, we note that

$$\frac{dD_{ij}}{dt} = \mathbf{n}_{ij} \cdot (\mathbf{v}(\mathbf{P}_i^{ij}) - \mathbf{v}(\mathbf{P}_j^{ij})) = \mathbf{n}_{ij} \cdot (A_{ij}\mathbf{u}) = N_{ij}A_{ij}\mathbf{u}.$$

Then, the founding NSCD algorithm [19, 18] choose to discretize the set of admissible velocities $\mathcal{C}_{\mathbf{c}}$ (2) using the following discrete constraint:

$$\forall \alpha \in I_c, \quad N_\alpha^k A_\alpha^k \mathbf{u}^{k+1} \geq 0 \quad \text{if} \quad D_\alpha^k \leq 0, \tag{8}$$

where the superscript k expresses the fact that the corresponding quantities have to be computed a time $k\Delta t$ (i.e. for the configuration $\mathbf{c}^k$). Such a discretization was also used in [39, 6]. Doing so, the constraint is implicit in the unknown velocity. However, for any α in I_c, if $D_\alpha^k > 0$, the corresponding non-overlapping constraint is not taken into account at time-step k and the time discretization can make D_α^{k+1} strictly negative so that the corresponding particles overlap. To stabilize the scheme, we follow [5, 27] and use a Taylor expansion of the constraint: the discrete constraint is written

$$D_\alpha^k + \Delta t\, N_\alpha^k A_\alpha^k \mathbf{u} \geq 0, \tag{9}$$

for α in I_c, and the discrete set of constraints is defined as

$$K^k = \left\{ \mathbf{u} \in \mathbb{R}^{6N} \quad \text{s.t.} \quad D_\alpha^k + \Delta t\, N_\alpha^k A_\alpha^k \mathbf{u} \geq 0\,,\ \alpha \in I_c \right\}. \tag{10}$$

In that case, the constraint is implicit again. It is a first order approximation of the non-overlapping constraints $D_\alpha^{k+1} \geq 0$ for $\alpha \in I_c$, the error being of order $O(\Delta t^2)$. Note that, in case of spherical particles, due to the convexity of the distance function, this constraint has the advantage to return feasible configurations (i.e. it avoids numerical interpenetration).

1.3.2 The corresponding velocity-based quadratic optimization problem with affine inequality constraints

The time-stepping algorithm proposed in [27] for spherical particles can be straightforwardly adapted to non spherical particles by considering the following problem: find $\mathbf{u} \in \mathbb{R}^{6N}$ solution to the minimization problem

$$(\mathcal{P}^k_{\min,\mathbf{u}}) \quad \left| \begin{array}{l} \min\limits_{\mathbf{u}\in K^k} J(\mathbf{u}), \\ J(\mathbf{u}) = \dfrac{1}{2}\left\|\mathbf{u} - \mathbf{U}^{k+1}\right\|_M^2, \quad \mathbf{U}^{k+1} = \mathbf{u}^k + \Delta t \mathbf{M}^{-1}\mathbf{F}^k, \\ K^k = \left\{\mathbf{u} \in \mathbb{R}^{6N}, \quad g_\alpha^k(\mathbf{u}) \leq 0\,,\ \alpha \in I_c\right\}, \\ g_\alpha^k(\mathbf{u}) = -D_\alpha^k - \Delta t\, N_\alpha^k A_\alpha^k \mathbf{u}. \end{array} \right. \tag{11}$$

where $\mathbf{F}^k = \mathbf{F}(\mathbf{u}^k)$ and $\|\mathbf{w}\|_{\mathbf{M}}$ is the $\mathbf{M}$-norm $\|\mathbf{w}\|_{\mathbf{M}}^2 := \mathbf{w} \cdot \mathbf{M}\mathbf{w}$. The vector $\mathbf{U}^{k+1}$ is the discrete free flight velocity: it is equal to the velocity that would be computed using an explicit Euler scheme without contact. The discrete problem (11) can be seen as a discretization of the continuous contact law (6): the particle velocity $\mathbf{u}^{k+1}$ is the projection of $\mathbf{U}^{k+1}$ on the discrete set of admissible velocities K^k.

For each time-step, solving the incremental problem amounts to minimize the convex functional J under the affine inequality constraints $g_\alpha^k \leq 0\,,\ \alpha \in I_c$. There exists a unique solution to this constrained minimization problem. Moreover, the constraints are qualified (finite number of affine constraints). Then, if $\mathbf{u}^{k+1}$ is solution to (11), there exists Lagrange multipliers $f_n^\alpha \geq 0\,,\ \alpha \in I_c$ such that the following Kuhn-Tucker optimality condition is verified:

$$\begin{aligned} &\nabla J(\mathbf{u}^{k+1}) = -\sum_{\alpha\in I_c} f_n^\alpha \nabla g_\alpha^k(\mathbf{u}^{k+1}), \\ &g_\alpha^k(\mathbf{u}^{k+1}) \leq 0, \quad f_n^\alpha \geq 0, \quad g_\alpha^k(\mathbf{u}^{k+1})\, f_n^\alpha = 0\,,\ \alpha \in I_c. \end{aligned} \tag{12}$$

Computing ∇J and ∇g_α, we obtain that these optimality conditions write

$$\begin{aligned}
&\mathbf{M}\,\frac{\mathbf{u}^{k+1}-\mathbf{u}^k}{\Delta t} = \mathbf{F}^k + \sum_{\alpha\in I_c} (N_\alpha^k A_\alpha^k)^T f_n^\alpha,\\
&\mathbf{D}^k + \Delta t\, N_\alpha^k A_\alpha^k \mathbf{u}^{k+1} \geq 0\,,\ f_n^\alpha \geq 0\,, \qquad \forall \alpha \in I_c,\\
&(\mathbf{D}^k + \Delta t\, N_\alpha^k A_\alpha^k \mathbf{u}^{k+1})\, f_n^\alpha = 0\,, \qquad \forall \alpha \in I_c.
\end{aligned}$$

Using (9), together with the fact that $(N_\alpha^k A_\alpha^k)^T f_n^\alpha = (A_\alpha^k)^T f_n^\alpha \mathbf{n}_\alpha^k$, one can see that these equations are a natural Euler-based time discretization of (4,5):

$$\begin{aligned}
&\mathbf{M}\,\frac{\mathbf{u}^{k+1}-\mathbf{u}^k}{\Delta t} = \mathbf{F}^k + \sum_{\alpha\in I_c} (A_\alpha^k)^T f_n^\alpha \mathbf{n}_\alpha^k,\\
&\mathbf{D}^k + \Delta t\, N_\alpha^k A_\alpha^k \mathbf{u}^{k+1} \geq 0\,,\ f_n^\alpha \geq 0\,, \qquad \forall \alpha \in I_c\\
&(\mathbf{D}^k + \Delta t\, N_\alpha^k A_\alpha^k \mathbf{u}^{k+1})\, f_n^\alpha = 0\,, \qquad \forall \alpha \in I_c.
\end{aligned} \tag{13}$$

This suggests that the solution to the model (4-7) can be approximated by solving the constrained convex problem $(\mathcal{P}^k_{\min,\mathbf{u}})$ (11) at each time-step . It has in fact been shown that the corresponding discrete solution converges towards the solution to the model when the time-step goes to zero (see [27] for a single contact and [9] for multiple contacts). Although one can expect a convergence with order 1 in Δt, the proofs of convergence in these papers are based on compactness methods and no theoretical results on the order of convergence of the algorithm are currently available.

1.3.3 The corresponding dual problem: maximization of a (discrete) global energy dissipation

In this section we detail the computations leading to the dual optimization problem. Indeed, an advantage of considering the dual problem is that in that case, the unknowns are the set of contact forces $(f_n^\alpha)_\alpha$ and the corresponding constraints are $f_n^\alpha \geq 0\,,\ \alpha \in I_c$. The projection on this new set of constraints is straightforward and many algorithms can take advantage of this explicit projection to solve the problem (see Section 3.1.1).

To begin, let us first define the following vectors and matrices:

$$\begin{aligned}
\mathbf{D} &= (D_\alpha\, \mathbf{n}_\alpha)_{\alpha\in I_c} \in \mathbb{R}^{3\,N(N-1)/2} \quad , \quad \mathbf{D}_n = (D_\alpha)_{\alpha\in I_c} \in \mathbb{R}^{N(N-1)/2},\\
\mathbf{A} &= \begin{pmatrix} \vdots \\ A_\alpha \\ \vdots \end{pmatrix}_{\alpha\in I_c} \in \mathcal{M}_{3\,N(N-1)/2\times 6N} \quad , \quad \mathbf{A}_n = \begin{pmatrix} \vdots \\ N_\alpha A_\alpha \\ \vdots \end{pmatrix}_{\alpha\in I_c} \in \mathcal{M}_{N(N-1)/2\times 6N}.
\end{aligned} \tag{14}$$

In the previous notations, the index n reflects the "normal" character of the quantity considered (e.g. the matrix $\mathbf{A}$ applied to a generalized velocity vector $\mathbf{u}$ provides the corresponding relative velocities at each contact point while $\mathbf{A}_n$ returns their normal coordinates).

The discrete space of admissible velocity in (11) can be rewritten as

$$K^k = \left\{\mathbf{u}\in\mathbb{R}^{6N},\quad \mathbf{g}^k(\mathbf{u}) \leq 0\right\}, \quad \mathbf{g}^k : \begin{array}{ccc} \mathbb{R}^{6N} & \to & \mathbb{R}^{N(N-1)/2} \\ \mathbf{u} & \mapsto & -\mathbf{D}_n^k - \Delta t \mathbf{A}_n^k \mathbf{u} \end{array}. \tag{15}$$

Let us now denote by $\boldsymbol{\lambda}_n \in \mathbb{R}^{N(N-1)/2}$ the vector of Lagrange multipliers corresponding to the $N(N-1)/2$ constraints ($\boldsymbol{\lambda}_n = (f_n^\alpha)_{\alpha\in I_c}$). The Lagrangian associated to the minimization problem (11) is:

$$\mathcal{L}(\mathbf{u}, \boldsymbol{\lambda}_n) = J(\mathbf{u}) + \boldsymbol{\lambda}_n \cdot (-\mathbf{D}_n^k - \Delta t \mathbf{A}_n^k \mathbf{u}).$$

The constraints being qualified, the duality theory says that

$$\inf_{\mathbf{u}\in K} J(\mathbf{u}) = \inf_{\mathbf{u}\in\mathbb{R}^{6N}} \sup_{\boldsymbol{\lambda}_n \geq 0} \mathcal{L}(\mathbf{u}, \boldsymbol{\lambda}_n) = \sup_{\boldsymbol{\lambda}_n \geq 0} \inf_{\mathbf{u}\in\mathbb{R}^{6N}} \mathcal{L}(\mathbf{u}, \boldsymbol{\lambda}_n),$$

so that the primal minimization problem (11) is equivalent to the following problem: find $\boldsymbol{\lambda}_n \in \mathbb{R}^{N(N-1)/2}$ solution to the dual maximization problem

$$\max_{\boldsymbol{\lambda}_n \in \bar{K}} \bar{J}(\boldsymbol{\lambda}_n), \tag{16}$$

with

$$\bar{J}(\boldsymbol{\lambda}_n) = \min_{\mathbf{u}\in\mathbb{R}^{6N}} \mathcal{L}(\mathbf{u},\boldsymbol{\lambda}_n)\,, \qquad \bar{K} = \left\{\boldsymbol{\lambda}_n \in \mathbb{R}^{N(N-1)/2}\,,\ \boldsymbol{\lambda}_n \geq 0\right\}.$$

Standard calculations allow to express explicitly the function $\boldsymbol{\lambda}_n \mapsto \bar{J}(\boldsymbol{\lambda}_n)$. First, $\boldsymbol{\lambda}_n$ being fixed, one can write the optimality condition for the unconstrained minimization problem and find $\mathbf{u}_{\boldsymbol{\lambda}_n}$ minimizing $\mathbf{u} \mapsto \mathcal{L}(\mathbf{u},\boldsymbol{\lambda}_n)$:

$$\mathbf{u}_{\boldsymbol{\lambda}_n} = \mathbf{U} + \Delta t \mathbf{M}^{-1}(\mathbf{A}_n^k)^T\boldsymbol{\lambda}_n.$$

Note that $\mathbf{u}_{\boldsymbol{\lambda}_n}$ is the velocity that would be computed using the discrete fundamental principle of dynamics (13) with contact forces $\boldsymbol{\lambda}_n$. From this, we can rewrite the dual problem as:

$$(\mathcal{P}^k_{\min,\boldsymbol{\lambda}}) \quad \left| \begin{array}{l} \min\limits_{\boldsymbol{\lambda}_n\in\bar{K}} \left(-\bar{J}(\boldsymbol{\lambda}_n)\right), \\ \bar{J}(\boldsymbol{\lambda}_n) = \mathcal{L}(\mathbf{u}_{\boldsymbol{\lambda}_n},\boldsymbol{\lambda}_n) = -\dfrac{\Delta t^2}{2}\boldsymbol{\lambda}_n^T\mathbf{A}_n^k\mathbf{M}^{-1}(\mathbf{A}_n^k)^T\boldsymbol{\lambda}_n - (\mathbf{D}_n + \Delta t\mathbf{A}_n^k\mathbf{U})^T\boldsymbol{\lambda}_n, \\ \bar{K} = \left\{\boldsymbol{\lambda}_n \in \mathbb{R}^{N(N-1)/2}\,,\ \boldsymbol{\lambda}_n \geq 0\right\}. \end{array} \right. \tag{17}$$

As mentioned before, the projection onto the set $\bar{K}$ is explicit and, therefore, several optimization solvers such as projected gradients are available to solve the problem.

Let us now show that problem $(\mathcal{P}^k_{\min,\boldsymbol{\lambda}})$ (17) can be seen as a global discrete mechanical energy minimization. Indeed, one can rewrite the functional up to constants independent of $\boldsymbol{\lambda}_n$ as (the superscripts k, as well as the subscript n in $\mathbf{u}_{\boldsymbol{\lambda}_n}$, are omitted for readability reasons):

$$\begin{aligned}
\bar{J}(\boldsymbol{\lambda}_n) &= \frac{1}{2}\mathbf{u}_{\boldsymbol{\lambda}}^T\mathbf{M}\mathbf{u}_{\boldsymbol{\lambda}} - \mathbf{U}^T\mathbf{M}\mathbf{u}_{\boldsymbol{\lambda}} + \boldsymbol{\lambda}_n^T(-\mathbf{D}_n - \Delta t\mathbf{A}_n\mathbf{u}_{\boldsymbol{\lambda}}) + cst \\
&= \frac{1}{2}\mathbf{u}_{\boldsymbol{\lambda}}^T\mathbf{M}(\mathbf{U} + \Delta t\mathbf{M}^{-1}\mathbf{A}_n^T\boldsymbol{\lambda}_n) - \mathbf{U}^T\mathbf{M}(\mathbf{U} + \Delta t\mathbf{M}^{-1}\mathbf{A}_n^T\boldsymbol{\lambda}_n) + \boldsymbol{\lambda}_n^T(-\mathbf{D}_n - \Delta t\mathbf{A}_n\mathbf{u}_{\boldsymbol{\lambda}}) + cst \\
&= \frac{1}{2}\mathbf{u}_{\boldsymbol{\lambda}}^T\mathbf{M}\mathbf{U} + \frac{1}{2}\Delta t\mathbf{u}_{\boldsymbol{\lambda}}^T\mathbf{A}_n^T\boldsymbol{\lambda}_n - \Delta t\mathbf{U}^T\mathbf{A}_n^T\boldsymbol{\lambda}_n + \boldsymbol{\lambda}_n^T(-\mathbf{D}_n - \Delta t\mathbf{A}_n\mathbf{u}_{\boldsymbol{\lambda}}) + cst \\
&= \frac{1}{2}(\mathbf{U} + \Delta t\mathbf{M}^{-1}\mathbf{A}_n^T\boldsymbol{\lambda}_n)^T\mathbf{M}\mathbf{U} + \frac{1}{2}\Delta t\mathbf{u}_{\boldsymbol{\lambda}}^T\mathbf{A}_n^T\boldsymbol{\lambda}_n - \Delta t\mathbf{U}^T\mathbf{A}_n^T\boldsymbol{\lambda}_n + \boldsymbol{\lambda}_n^T(-\mathbf{D}_n - \Delta t\mathbf{A}_n\mathbf{u}_{\boldsymbol{\lambda}}) + cst \\
&= \frac{1}{2}\Delta t(\mathbf{M}^{-1}\mathbf{A}_n^T\boldsymbol{\lambda}_n)^T\mathbf{M}\mathbf{U} + \frac{1}{2}\Delta t\mathbf{u}_{\boldsymbol{\lambda}}^T\mathbf{A}_n^T\boldsymbol{\lambda}_n - \Delta t\mathbf{U}^T\mathbf{A}_n^T\boldsymbol{\lambda}_n + \boldsymbol{\lambda}_n^T(-\mathbf{D}_n - \Delta t\mathbf{A}_n\mathbf{u}_{\boldsymbol{\lambda}}) + cst \\
&= \frac{1}{2}\Delta t\boldsymbol{\lambda}_n^T\mathbf{A}_n\mathbf{U} + \frac{1}{2}\Delta t\boldsymbol{\lambda}_n^T\mathbf{A}_n\mathbf{u}_{\boldsymbol{\lambda}} - \Delta t\boldsymbol{\lambda}_n^T\mathbf{A}_n\mathbf{U} - \boldsymbol{\lambda}_n^T\mathbf{D}_n - \Delta t\boldsymbol{\lambda}_n^T\mathbf{A}_n\mathbf{u}_{\boldsymbol{\lambda}} + cst.
\end{aligned}$$

Then, we have:

$$-\bar{J}(\boldsymbol{\lambda}_n) = \boldsymbol{\lambda}_n^T\left[\mathbf{D}_n^k + \Delta t\mathbf{A}_n^k\left(\frac{\mathbf{u}_{\boldsymbol{\lambda}_n}+\mathbf{U}}{2}\right)\right] + cst = \sum_{\alpha\in I_c} f_n^\alpha\left[D_\alpha^k + \Delta t N_\alpha^k A_\alpha^k\left(\frac{\mathbf{u}_{\boldsymbol{\lambda}_n}+\mathbf{U}}{2}\right)\right] + cst. \tag{18}$$

The functional to minimize corresponds to a discrete energy, dissipated by the normal contact forces $\boldsymbol{\lambda}_n = (f_n^\alpha)_\alpha$ for relative velocities computed from the mean of the free-flight velocity $\mathbf{U}$ and the real velocity $\mathbf{u}_{\boldsymbol{\lambda}_n}$. Then, the solution to the numerical scheme both satisfies the discrete fundamental principle of dynamics (13) at each contact point and minimizes a global discrete energy over all the contacts. This discrete energy is in agreement with the models proposed by Frémond in [14] or [15, Chap.8], where the expression of virtual work involves the term $m(\mathbf{u}^+ - \mathbf{u}^-)\cdot(\mathbf{v}^+ + \mathbf{v}^-)/2$ with $\mathbf{u}$ the actual velocity and $\mathbf{v}$ the virtual one. In (18), $\mathbf{U}$ stands for the pre-impact velocity, $\mathbf{u}_{\boldsymbol{\lambda}_n}$ the post-impact velocity, and the instantaneous contact force f is related to the momentum jump $m(\mathbf{u}^+ - \mathbf{u}^-)$ by the fundamental principle of dynamics at the instant of contact.

2 Convex schemes for frictional contacts

In this section, we present how the previous computations can be extended to design convex algorithms in the frictional case. After stating the problem and the corresponding non-convex natural time-stepping scheme, we present two schemes proposed in the literature and based on convex problems. The first one is a convex relaxation of the natural discrete problem, leading to a convex minimization problem under conic constraints [4, 43, 7, 26]. The second one proposes to solve the non-convex problem using a fixed point method [2] in which each iteration reduces to an iteration of the type of the relaxed scheme. As in the frictionless case, we prove that the corresponding incremental problem can be understood as the minimization of a global energy.

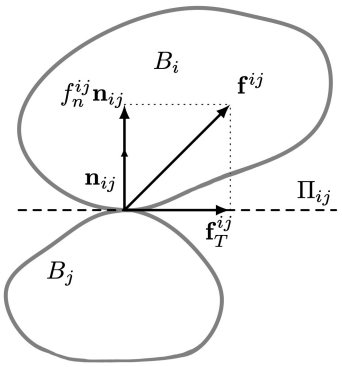

Figure 2: Notations: force decomposition

2.1 Modeling friction

Due to friction, the contact force $\mathbf{f}^\alpha$ is no longer colinear to $\mathbf{n}_\alpha$:

$$\mathbf{f}^\alpha = f_n^\alpha \mathbf{n}_\alpha + \mathbf{f}_T^\alpha,$$

where $f_n^\alpha = N_\alpha \mathbf{f}^\alpha$ is the normal component of the force along $\mathbf{n}_\alpha$ and $\mathbf{f}_T^\alpha = T_\alpha \mathbf{f}^\alpha$ is its tangential part (projection onto Π_α, the tangent plane to the surface, see Figure 2).

To model frictional contact, one has to describe the contact law. The normal contact law is still driven by the non-overlapping constraint: the Signorini conditions (1) together with the contact law (2) have to be satisfied. As for the tangential contact law, we consider *Coulomb's law*. For any $\alpha \in I_c$, the contact force must belong to the so-called Coulomb cone:

$$\begin{aligned} \mathcal{C}_{\mu,\alpha}^{\text{Coulomb}} &= \left\{ \mathbf{f} \in \mathbb{R}^3 \text{ s.t. } | T_\alpha A_\alpha \mathbf{f} | \leq \mu N_\alpha A_\alpha \mathbf{f} \right\} \\ &= \left\{ \mathbf{f} \in \mathbb{R}^3 \text{ s.t. } | \mathbf{f}_T^\alpha | \leq \mu f_n^\alpha \right\}, \end{aligned} \tag{19}$$

where μ is the friction coefficient and depends on the physical properties of the surfaces. In case of a sliding motion ($N_\alpha A_\alpha \mathbf{v}^+ \neq 0$), the force has to belong to the boundary of Coulomb cone and must be oriented in the opposite direction to the relative tangential velocity. The tangential contact law can then be written as: for any $\alpha \in I_c$,

$$\begin{aligned} &\text{If } T_\alpha A_\alpha \mathbf{u}^+ \neq 0 \text{ (sliding motion)}, \ \mathbf{f}_T^\alpha = -\mu f_n^\alpha \frac{T_\alpha A_\alpha \mathbf{u}^+}{| T_\alpha A_\alpha \mathbf{u}^+ |}, \\ &\text{If } T_\alpha A_\alpha \mathbf{u}^+ = 0 \text{ (no slip)}, \ | \mathbf{f}_T^\alpha | \leq \mu f_n^\alpha. \end{aligned}$$

The equations of motion now write, in the sense of distributions or measures:

$$\frac{d\mathbf{c}}{dt} = \mathcal{L}(\mathbf{u}), \tag{20}$$

$$\mathbf{M}\frac{d\mathbf{u}}{dt} = \mathbf{F}(\mathbf{u}) + \sum_{\alpha \in I_c} A_\alpha^T (f_n^\alpha \mathbf{n}_\alpha + \mathbf{f}_T^\alpha), \tag{21}$$

$$D_\alpha(\mathbf{c}) \geq 0, \ f_n^\alpha \geq 0, \ D_\alpha(\mathbf{c})\, f_n^\alpha = 0, \ \forall \alpha \in I_c, \tag{22}$$

$$\mathbf{u}^+ = P_{\mathcal{C}_\mathbf{c}} \mathbf{u}^-, \tag{23}$$

$$\text{If } T_\alpha A_\alpha \mathbf{u}^+ \neq 0 \text{ (sliding motion)}, \ \mathbf{f}_T^\alpha = -\mu f_n^\alpha \frac{T_\alpha A_\alpha \mathbf{u}^+}{| T_\alpha A_\alpha \mathbf{u}^+ |}, \ \forall \alpha \in I_c, \tag{24}$$

$$\text{If } T_\alpha A_\alpha \mathbf{u}^+ = 0 \text{ (no slip)}, \ | \mathbf{f}_T^\alpha | \leq \mu f_n^\alpha, \ \forall \alpha \in I_c, \tag{25}$$

$$\mathbf{c}(0) = \mathbf{c}_0, \quad \mathbf{u}(0) = \mathbf{u}_0. \tag{26}$$

2.2 Convex numerical schemes: a second-order cone constraint

2.2.1 A non-convex natural Euler-based time-stepping discretization

As in the previous section, one can follow [19, 18, 39, 6], and discretize the normal constraint using (8). Here, following again [27] and [5], we consider the Taylor expansion of the constraint (10) in order to stabilize the

scheme. Then, to solve (21,25), a natural Euler-based time-stepping discretization is

$$\left|\begin{array}{l}
\mathbf{M}\,\dfrac{\mathbf{u}^{k+1}-\mathbf{u}^k}{\Delta t} = \mathbf{F}^k + \displaystyle\sum_{\alpha\in I_c} (A_\alpha^k)^T (f_n^\alpha \mathbf{n}_\alpha^k + \mathbf{f}_T^\alpha),\\
\mathbf{D}_n^k + \Delta t\, N_\alpha^k A_\alpha^k \mathbf{u}^{k+1} \geq 0\,,\ f_n^\alpha \geq 0\,, \qquad \forall \alpha \in I_c,\\
(\mathbf{D}_n^k + \Delta t\, N_\alpha^k A_\alpha^k \mathbf{u}^{k+1})\, f_n^\alpha = 0\,, \qquad \forall \alpha \in I_c,\\
\text{If } T_\alpha A_\alpha \mathbf{u}^{k+1} \neq 0 \text{ (sliding motion)}\,,\ \mathbf{f}_T^\alpha = -\mu f_n^\alpha \dfrac{T_\alpha A_\alpha \mathbf{u}^{k+1}}{|\, T_\alpha A_\alpha \mathbf{u}^{k+1}\,|}\,, \qquad \forall \alpha \in I_c,\\
\text{If } T_\alpha A_\alpha \mathbf{u}^{k+1} = 0 \text{ (no slip)}\,,\ |\,\mathbf{f}_T^\alpha\,| \leq \mu f_n^\alpha\,, \qquad \forall \alpha \in I_c.
\end{array}\right. \tag{27}$$

Although this scheme is stable, it requires solving, at each time-step, a non-convex Linear Complementarity Problem which proves to be expensive to solve. As stated in the introduction, the most widely spread numerical strategies to compute the corresponding solutions are based on projection/splitting methods, Gauss-Seidel like relaxations or generalized Newton methods. Unfortunately, no convergence result for the corresponding iterative methods are available.

2.2.2 A relaxed scheme based on a quadratic optimization problem with second-order cone constraints

To make the problem easier to solve, one can follow the idea of the frictionless algorithm and search for a time discretization leading to a convex constrained optimization problem to be solved at each time-step. To do so, one should find an optimization problem for which the optimality conditions are discretization of (21,25), the contact forces being the corresponding Lagrange multipliers. Note that, in order to obtain an optimality constraint for which the Lagrange multipliers belong to a cone, one now has to consider non-differentiable constraints (of conic type) and substitute the notion of sub-differential of a function for that of gradient. We refer the reader who is not used to handling sub-differentials to appendix A where the notion is introduced and the computations are detailed.

So let us consider the following minimization problem:

$$(\mathcal{P}^k_{\min,\mu,\mathbf{u}}) \quad \left|\begin{array}{l}
\displaystyle\min_{\mathbf{u}\in K_\mu^k} J(\mathbf{u}),\\
J(\mathbf{u}) = \dfrac{1}{2}\left\|\mathbf{u}-\mathbf{U}^{k+1}\right\|_M^2\,, \quad \mathbf{U}^{k+1} = \mathbf{u}^k + \Delta t \mathbf{M}^{-1}\mathbf{F}^k,\\
K_\mu^k = \left\{\mathbf{u}\in\mathbb{R}^{6N}, \quad g_{\alpha,\mu}^k(\mathbf{u}) \leq 0\,,\ \alpha \in I_c\right\},\\
g_{\alpha,\mu}^k(\mathbf{u}) = -D_\alpha^k - \Delta t\, N_\alpha^k A_\alpha^k \mathbf{u} + \mu\Delta t \left|\, T_\alpha^k A_\alpha^k \mathbf{u}\,\right|,
\end{array}\right. \tag{28}$$

and show that the corresponding optimality conditions are a formal discretization of (21,25).

If $\mathbf{u}^{k+1}$ is solution to (28), and *if the contraints are qualified* (see discussion below), there exists Lagrange multipliers $f_n^\alpha \geq 0\,,\ \alpha \in I_c$ such that the following Kuhn-Tucker optimality condition is verified (counterpart of (12) in the non-differentiable case):

$$\begin{array}{l}
\nabla J(\mathbf{u}^{k+1}) \in -\displaystyle\sum_{\alpha\in I_c} f_n^\alpha \partial g_{\alpha,\mu}^k[\mathbf{u}^{k+1}],\\
g_{\alpha,\mu}^k(\mathbf{u}^{k+1}) \leq 0, \quad f_n^\alpha \geq 0, \quad g_{\alpha,\mu}^k(\mathbf{u}^{k+1})\, f_n^\alpha = 0\,,\ \alpha \in I_c.
\end{array} \tag{29}$$

where $\partial g_{\alpha,\mu}^k[\mathbf{u}]$ denotes the sub-differential of function $g_{\alpha,\mu}^k$ at point $\mathbf{u}$.

In general, sub-differentials cannot be summed. However, in our case, $g_{\alpha,\mu}^k$ is the sum of a differentiable part (for which the sub-differential contains a unique point which is the gradient) and a non-differentiable part. In that case, the two sub-differential can be summed and we have (see appendix A):

$$\begin{array}{l}
\text{If } T_\alpha^k A_\alpha^k \mathbf{u} \neq 0, \quad \partial g_{\alpha,\mu}[\mathbf{u}] = \left\{ \Delta t (A_\alpha^k)^T \left(-\mathbf{n}_\alpha^k + \mu \dfrac{T_\alpha^k A_\alpha^k \mathbf{u}}{|\, T_\alpha^k A_\alpha^k \mathbf{u}\,|} \right) \right\},\\
\text{If } T_\alpha^k A_\alpha^k \mathbf{u} = 0, \quad \partial g_{\alpha,\mu}[\mathbf{u}] = \left\{ \Delta t (A_\alpha^k)^T \left(-\mathbf{n}_\alpha^k + \mu \mathbf{w} \right) \ / \ \mathbf{w} \in \Pi_\alpha^k \text{ and } |\,\mathbf{w}\,| \leq 1 \right\},
\end{array}$$

where Π_α^k is the tangent plane to the surfaces for contact α at step k. From this, the optimality condition for (28) can be written as

$$
\begin{aligned}
& M\,\frac{\mathbf{u}^{k+1}-\mathbf{u}^k}{\Delta t} = \mathbf{F}^{ext} + \sum_{\alpha\in I_c} (A_\alpha^k)^T (f_n^\alpha \mathbf{n}_\alpha^k - \mu f_n^\alpha \mathbf{w}),\\
& f_n^\alpha \geq 0, \quad g_{\alpha,\mu}(\mathbf{u}^{k+1}) \leq 0, \quad f_n^\alpha\, g_{\alpha,\mu}(\mathbf{u}^{k+1}) = 0\,, \qquad \forall \alpha \in I_c,\\
& \text{If } T_\alpha^k A_\alpha^k \mathbf{u}^{k+1} \neq 0 \text{ (sliding motion)}, \quad \mathbf{w} = \frac{T_\alpha^k A_\alpha^k \mathbf{u}^{k+1}}{|\, T_\alpha^k A_\alpha^k \mathbf{u}^{k+1}\,|}\,, \qquad \forall \alpha \in I_c,\\
& \text{If } T_\alpha^k A_\alpha^k \mathbf{u}^{k+1} = 0 \text{ (no slip)}\,, \quad \mathbf{w} \in \Pi_\alpha^k \text{ and } |\,\mathbf{w}\,| \leq 1\,, \qquad \forall \alpha \in I_c.
\end{aligned}
$$

Setting the tangential forces as $\mathbf{f}_T^\alpha = -\mu f_n^\alpha \mathbf{w}$, we finally obtain that $\mathbf{u}^{k+1}$ is solution to the discrete problem

$$
(\mathcal{P}^k_{\mathrm{CCP},\mu}) \quad \left|
\begin{aligned}
& \mathbf{M}\,\frac{\mathbf{u}^{k+1}-\mathbf{u}^k}{\Delta t} = \mathbf{F}^k + \sum_{\alpha\in I_c} (A_\alpha^k)^T (f_n^\alpha \mathbf{n}_\alpha^k + \mathbf{f}_T^\alpha),\\
& D_\alpha^k + \Delta t\, N_\alpha^k A_\alpha^k \mathbf{u}^{k+1} \geq \mu \Delta t \left|\, T_\alpha^k A_\alpha^k \mathbf{u}^{k+1}\,\right|\,,\ f_n^\alpha \geq 0\,, \qquad \forall \alpha \in I_c,\\
& \left(D_\alpha^k + \Delta t\, N_\alpha^k A_\alpha^k \mathbf{u}^{k+1} - \mu \Delta t \left|\, T_\alpha^k A_\alpha^k \mathbf{u}^{k+1}\,\right|\right) f_n^\alpha = 0\,, \qquad \forall \alpha \in I_c,\\
& \text{If } T_\alpha^k A_\alpha^k \mathbf{u}^{k+1} \neq 0 \text{ (sliding motion)}\,,\ \mathbf{f}_T^\alpha = -\mu f_n^\alpha \frac{T_\alpha^k A_\alpha^k \mathbf{u}^{k+1}}{|\, T_\alpha^k A_\alpha^k \mathbf{u}^{k+1}\,|}\,, \qquad \forall \alpha \in I_c,\\
& \text{If } T_\alpha^k A_\alpha^k \mathbf{u}^{k+1} = 0 \text{ (no slip)}\,,\ |\,\mathbf{f}_T^\alpha\,| \leq \mu f_n^\alpha\,, \qquad \forall \alpha \in I_c,
\end{aligned}
\right. \tag{30}
$$

which is a (formal) discretization of the continuous frictional problem (21,25).

Let us now discuss the fact that the existence of Lagrange multipliers leading to this problem is subject to the aforementioned *constraint qualification* condition. Checking this qualification condition amounts to show that the interior of the feasible set K_μ^k (28) is not empty. If the non-empty character of K_μ^k is assured in many situations, the existence of a point belonging to its interior is not obvious in general. In the case of a single contact, it is ensured by the choice of velocities leading to a relative velocity oriented along the normal to the contact point (whatever the shape of the particles). The qualification of the constraint can also be proved in the case of granular media made of N spherical particles. Indeed, in that case, the velocity vector

$$\mathbf{u}_0 = (\epsilon \mathbf{c}_1, 0, \epsilon \mathbf{c}_2, 0, \ldots, \epsilon \mathbf{c}_N, 0)$$

do not generate tangential relative velocities and lies in the interior of K_μ^k for $\epsilon > 0$. In the multi-particle case, with more general particle shapes, it may be necessary to suppose that $\mu\Delta t$ is sufficiently small, in order to relax the constraint and obtain its qualification.

Thus, provided that the constraints are qualified, one can choose to approximate the solution to the frictional model (21) by solving the CCP problem $(\mathcal{P}^k_{\mathrm{CCP},\mu})$ (30) or the constrained minimization problem $(\mathcal{P}^k_{\min,\mu,\mathbf{u}})$ (28). The first strategy is followed in [4] where the Coulomb cone is approximated by a faceted discretization or in [43, 7] where a Gauss-Seidel-like iterative method proved to converge under assumptions on the configuration of the system is implemented. The second strategy is followed in [26] where the constrained minimization problem is solved using an interior point method.

To finish this section, let us say that, as stated in the introduction, very few results of convergence in Δt are available for these schemes. One can cite [40] where the convergence of the non-convex scheme is proved for a single contact problem and a faceted approximation of Coulomb cone. In [4] a convergence result for the convex CCP scheme (30) is stated. Again the faceted cone is considered and the limit solutions are proved to satisfy the fundamental principle of dynamics with forces belonging to the faceted cone. Obtaining convergence to the limit contact laws in the multi-particle case is a particularly tricky problem that has not yet been addressed. Moreover, none of the existing results provides an error estimate as a function of the time-step.

2.2.3 The corresponding dual problem: maximization of a (discrete) global dissipation under conic constraint

As in the frictionless case, it may be convenient to solve the dual discrete problem instead of $(\mathcal{P}^k_{\min,\mu,\mathbf{u}})$ (28). We prove in this section that this dual problem can again be seen as a global energy minimization problem. More precisely, we propose a frictional counterpart of the frictionless energy $-\bar{J}$ (18), based again on the mean of the free-flight and actual velocities, and show that (30) are the corresponding optimality conditions.

Let us denote by $\boldsymbol{\lambda} = (\mathbf{f}^\alpha)_{\alpha \in I_c}$ the set of unknown forces and $\mathbf{u}_\lambda$ the corresponding velocity given by the discrete fundamental principle of dynamics at step k:

$$\mathbf{u}_{\boldsymbol{\lambda}} = \mathbf{U} + \Delta t \mathbf{M}^{-1} (\mathbf{A}^k)^T \boldsymbol{\lambda}, \tag{31}$$

where $\mathbf{A}^k$ was defined in (14).

By analogy with the frictionless case ($\mathcal{P}^k_{\text{min},\boldsymbol{\lambda}}$) (17,18), and following again Frémond (see [14] or [15, Chap.8]), we define the discrete energy as:

$$\begin{aligned}
\bar{G}(\boldsymbol{\lambda}) &= \sum_{\alpha \in I_c} f_n^\alpha \left[D_\alpha^k + \Delta t N_\alpha^k A_\alpha^k \left(\frac{\mathbf{u}_{\boldsymbol{\lambda}} + \mathbf{U}}{2} \right) \right] + \sum_{\alpha \in I_c} \left\langle \mathbf{f}_T^\alpha, \Delta t T_\alpha^k A_\alpha^k \left(\frac{\mathbf{u}_{\boldsymbol{\lambda}} + \mathbf{U}}{2} \right) \right\rangle \\
&= \sum_{\alpha \in I_c} \left\langle \mathbf{f}^\alpha, D_\alpha^k \mathbf{n}_\alpha^k + \Delta t A_\alpha^k \left(\frac{\mathbf{u}_{\boldsymbol{\lambda}} + \mathbf{U}}{2} \right) \right\rangle \\
&= \boldsymbol{\lambda}^T \left[\mathbf{D}^k + \Delta t \mathbf{A}^k \left(\frac{\mathbf{u}_{\boldsymbol{\lambda}} + \mathbf{U}}{2} \right) \right] \\
&= \frac{\Delta t^2}{2} \boldsymbol{\lambda}^T \mathbf{A}^k \mathbf{M}^{-1} (\mathbf{A}^k)^T \boldsymbol{\lambda} + (\mathbf{D}^k + \Delta t \mathbf{A}^k \mathbf{U})^T \boldsymbol{\lambda}.
\end{aligned}$$

For each α in I_c, the unknown force $\mathbf{f}^\alpha$ have to belong to the Coulomb cone $\mathcal{C}^{\text{Coulomb}}_{\mu,\alpha}$ defined in (19). Then we consider the following dual minimization problem

$$(\mathcal{P}^k_{\text{min},\mu,\boldsymbol{\lambda}}) \quad \left| \begin{array}{l} \min\limits_{\boldsymbol{\lambda} \in \bar{K}_\mu} \bar{G}(\boldsymbol{\lambda}), \\ \bar{G}(\boldsymbol{\lambda}_n) = \dfrac{\Delta t^2}{2} \boldsymbol{\lambda}^T \mathbf{A}^k \mathbf{M}^{-1} (\mathbf{A}^k)^T \boldsymbol{\lambda} + (\mathbf{D}^k + \Delta t \mathbf{A}^k \mathbf{U})^T \boldsymbol{\lambda}, \\ \bar{K}_\mu = \left\{ \boldsymbol{\lambda} = (\mathbf{f}^\alpha)_\alpha \in \mathbb{R}^{3N(N-1)/2}, \ h_\mu(\mathbf{f}^\alpha) \leq 0, \ \forall \alpha \in I_c \right\}, \\ h_\mu(\mathbf{f}^\alpha) = |\, \mathbf{f}_T^\alpha \,| - \mu f_n^\alpha. \end{array} \right. \tag{32}$$

Solving this dual problem has several advantages. First, although it again consists of a convex minimization problem under conic constraints, it is now easier to show that the constraints are qualified. Indeed, while the constraints of the primal problem ($\mathcal{P}^k_{\text{min},\mu,\mathbf{u}}$) are cross-dependent in the multi-particle case (changing the velocity of one of the particles modifies all the constraints linked to this particle), in the dual problem, all constraints are independent. Finding a point in the interior of the admissible set can be achieved for example by choosing $\mathbf{f}_T^\alpha = 0$ and $f_n^\alpha > 0$ for any α in I_c. Another advantage of the dual problem is that, as for the inelastic case ($\mathcal{P}^k_{\text{min},\boldsymbol{\lambda}}$), the projection onto the set of admissible forces is explicit and one can then solve the problem using for example projected gradient like algorithms.

Let us now show that any solution to this problem provides a solution to ($\mathcal{P}^k_{\text{CCP},\mu}$). The constraints being qualified, the optimality conditions writes (see again appendix A if needed): if $\boldsymbol{\lambda}$ is solution to ($\mathcal{P}^k_{\text{min},\mu,\boldsymbol{\lambda}}$), there exists Lagrange multipliers $(\gamma_\alpha)_{\alpha \in I_c}$ such that:

$$\begin{aligned}
&\nabla \bar{G}(\boldsymbol{\lambda}) \in - \sum_{\alpha \in I_c} \gamma_\alpha \partial h_\mu[\boldsymbol{\lambda}], \\
&h_\mu(\mathbf{f}^\alpha) \leq 0, \quad \gamma_\alpha \geq 0, \quad h_\mu(\mathbf{f}^\alpha)\, \gamma_\alpha = 0, \ \alpha \in I_c.
\end{aligned} \tag{33}$$

Let us prove that this set of equations implies that $\mathbf{u}_{\boldsymbol{\lambda}}$ defined in (31) is solution to ($\mathcal{P}^k_{\text{CCP},\mu}$) with the set of forces $\boldsymbol{\lambda} = (\mathbf{f}^\alpha)_\alpha$. By definition, $\mathbf{u}_{\boldsymbol{\lambda}}$ satisfies the discrete fundamental principle of dynamics for this set of forces. So it remains to show that the discrete constraint, complementarity condition and tangential contact laws are satisfied. First, we have

$$\begin{aligned}
\nabla \bar{G}(\boldsymbol{\lambda}) &= \Delta t^2 \mathbf{A}^k \mathbf{M}^{-1} (\mathbf{A}^k)^T \boldsymbol{\lambda} + (\mathbf{D}^k + \Delta t \mathbf{A}^k \mathbf{U}) \\
&= \Delta t^2 \left(\frac{1}{\Delta t} \mathbf{A}^k (\mathbf{u}_{\boldsymbol{\lambda}} - \mathbf{U}) \right) + (\mathbf{D}^k + \Delta t \mathbf{A}^k \mathbf{U}) \\
&= \mathbf{D}^k + \Delta t \mathbf{A}^k \mathbf{u}_{\boldsymbol{\lambda}}.
\end{aligned}$$

Then, computing the subdifferential of h_μ, we can write the optimality condition (33) as: for all α in I_c,

there exists $\mathbf{v}_\alpha \in \mathbb{R}^3$ with

$$D_\alpha^k \mathbf{n}_\alpha^k + \Delta t\, A_\alpha^k \mathbf{u}_{\boldsymbol{\lambda}} = -\gamma_\alpha(\mathbf{v}_\alpha - \mu \mathbf{n}_\alpha^k), \tag{34}$$

$$h_\mu(\mathbf{f}^\alpha) \leq 0, \quad \gamma_\alpha \geq 0, \quad h_\mu(\mathbf{f}^\alpha)\,\gamma_\alpha = 0, \tag{35}$$

$$\text{If } \mathbf{f}_T^\alpha \neq 0, \mathbf{v}_\alpha = -\frac{\mathbf{f}_T^\alpha}{|\,\mathbf{f}_T^\alpha\,|}, \tag{36}$$

$$\text{If } \mathbf{f}_T^\alpha = 0, \mathbf{v}_\alpha \in \Pi_\alpha^k\,,\ |\,\mathbf{v}_\alpha\,| \leq 1, \tag{37}$$

where we recall that Π_α^k is the tangent plane to the surfaces for contact α at time-step k. Projecting equation (34) on $\mathbf{n}_\alpha^k$ and Π_α^k we obtain that

$$\begin{aligned} \gamma_\alpha &= \frac{1}{\mu}\left[D_\alpha^k + \Delta t\, N_\alpha^k A_\alpha^k \mathbf{u}_{\boldsymbol{\lambda}}\right], \\ -\gamma_\alpha \mathbf{v}_\alpha &= \Delta t\, T_\alpha^k A_\alpha^k \mathbf{u}_{\boldsymbol{\lambda}}. \end{aligned} \tag{38}$$

This, together with $|\,\gamma_\alpha \mathbf{v}_\alpha\,| \geq \gamma_\alpha$ gives the discrete constraint for $\mathbf{u}_{\boldsymbol{\lambda}}$. The discrete contact law comes from (36,37). It then remains to prove the discrete complementarity condition. To do so, let us suppose that $D_\alpha^k + \Delta t\, N_\alpha^k A_\alpha^k \mathbf{u}_{\boldsymbol{\lambda}} > \mu \Delta t \left|\, T_\alpha^k A_\alpha^k \mathbf{u}_{\boldsymbol{\lambda}} \,\right|$ and show that $f_n^\alpha = 0$. In that case, from (38) we see that $|\,\mathbf{v}_\alpha\,| < 1$ and then from (36,37) we obtain $\mathbf{f}_T^\alpha = 0$. But we also have that $\gamma_\alpha = (D_\alpha^k + \Delta t\, N_\alpha^k A_\alpha^k \mathbf{u}_{\boldsymbol{\lambda}})/\mu > 0$ so from (35), $h_\mu(\mathbf{f}^\alpha) = 0$ and $f_n^\alpha = \mu\,|\,\mathbf{f}_T^\alpha\,| = 0$ which ends the proof.

2.2.4 Coupling with a fixed-point scheme

One of the drawbacks of the convex relaxation $g_{\alpha,\mu}^k(\mathbf{u}) \leq 0$ of the constraint in problem $(\mathcal{P}_{\min,\mu,\mathbf{u}}^k)$ (28) is that the non-overlapping constraint is over-estimated:

$$\mathbf{D}_n^k + \Delta t\, N_\alpha^k A_\alpha^k \mathbf{u}^{k+1} \geq \mu \Delta t \left|\, T_\alpha^k A_\alpha^k \mathbf{u}^{k+1} \,\right| > 0.$$

Although the error is controlled by Δt, this can lead to an undesired numerical dilatation of the medium (for example for large values of μ or large tangential velocities).

To avoid this problem, the authors in [2] propose to couple the convexification with a fixed-point formulation. They consider the convexified problem $(\mathcal{P}_{\min,\mu,\mathbf{u}}^k)$ or equivalently $(\mathcal{P}_{\mathrm{CCP},\mu}^k)$, introduce a new vector of parameters $\mathbf{s} = (s_\alpha)_\alpha \in \mathbb{R}^{N(N-1)/2}$ and modify the constraint as:

$$\mathbf{D}_n^k + \Delta t\, N_\alpha^k A_\alpha^k \mathbf{u}^{k+1} \geq \mu \Delta t (\left|\, T_\alpha^k A_\alpha^k \mathbf{u}^{k+1} \,\right| - s_\alpha)\,, \quad \forall \alpha \in I_c. \tag{39}$$

If $\mathbf{u}_{\mathbf{s}}^{k+1}$ is solution to this parameterized problem, they consider:

$$\begin{array}{rccc} F^k\ : & \mathbb{R}^{N(N-1)/2} & \to & \mathbb{R}^{N(N-1)/2} \\ & \mathbf{s} & \mapsto & \left(\left|\, T_\alpha^k A_\alpha^k \mathbf{u}_{\mathbf{s}}^{k+1} \,\right|\right)_{\alpha \in I_c} \end{array}$$

and search for a fixed point of this functional:

$$(\mathcal{P}_{\mathrm{FP},\mu,\boldsymbol{\lambda}}^k) \quad \left| \begin{array}{l} \text{Find } \mathbf{s} \text{ in } \mathbb{R}^{N(N-1)/2} \text{ s.t.} \\ \quad F^k(\mathbf{s}) = \mathbf{s} \end{array} \right. \tag{40}$$

Indeed, if $\mathbf{s}^\star$ is a fixed point of F^k, one has $s_\alpha^\star = \left|\, T_\alpha^k A_\alpha^k \mathbf{u}_{\mathbf{s}^\star}^{k+1} \,\right|$ for any $\alpha \in I_c$ and then, the constraint (39) for $\mathbf{u}_{\mathbf{s}^\star}^{k+1}$ is reduced to $\mathbf{D}_n^k + \Delta t\, N_\alpha^k A_\alpha^k \mathbf{u}_{\mathbf{s}^\star}^{k+1} \geq 0$ and $\mathbf{u}_{\mathbf{s}^\star}^{k+1}$ solves the non-convex discrete incremental problem (27). The existence of a fixed point is proved under the same assumptions as those necessary for the qualification of the constraint in the convexified problem (interior of the feasible set K_μ^k (28) not empty).

3 Numerical tests

In this section, we study the behavior of the different methods we have presented. If the behavior of the algorithms for solving the incremental (convex) problem has already been studied, we also present here a numerical study of convergence when the time-step tends to zero for the different dicretization schemes. In particular, we show in a simple case, for which an explicit solution can be computed, that each of the schemes converges with order 1 in Δt. In the case with friction, we also study the influence of the constraint convexification on the macroscopic behavior of the system. We show that, although it induces a numerical dilation effect, the profiles obtained in the case of a granular collapse are similar to those obtained without convexification, via the fixed point method. The numerical tests are run with the code SCoPI developped at CMAP laboratory [22].

3.1 Numerical algorithms to solve the discrete incremental problems

For each of the previously described methods, solving at each time-step the incremental problem turns back to solving a convex problem: $(\mathcal{P}^k_{\min,\mathbf{u}})$ or $(\mathcal{P}^k_{\min,\boldsymbol{\lambda}})$ without friction (see (11) or (17)) and the convexified problems $(\mathcal{P}^k_{\min,\mu,\mathbf{u}})$ or $(\mathcal{P}^k_{\min,\mu,\boldsymbol{\lambda}})$ with friction (see (28) or (32)). When using the fixed point method $(\mathcal{P}^k_{\mathrm{FP},\mu,\boldsymbol{\lambda}})$ (see (40)), one also has to solve, at each iteration of the fixed point method, a problem similar to the convexified frictional formulations. The main advantage of these formulations is that several methods are available to solve the convex problems.

3.1.1 Available numerical algorithms

First, one can use the optimality conditions leading to the CCP formulation $(\mathcal{P}^k_{\mathrm{CCP},\mu})$ (see (30)). Some authors have proposed an approach based on this formulation, using Projected Jacobi and Gauss-Seidel Jacobi methods [43, 7, 41, 42]. These methods require several iterations on the potential contacts and are known to become prohibitive for a large number of particles and contacts. A method that is also often used for problems with friction is to approximate Coulomb cone by a faceted cone, leading to a classical quadratic program (see e.g. [39, 38, 4]). Note that in 2d, Coulomb cone is actually a faceted cone.

More efficient strategies can be used, taking advantage of the convex minimization formulations. A first strategy consists in using the fact that, for the force-based minimization problems $(\mathcal{P}^k_{\min,\boldsymbol{\lambda}})$ and $(\mathcal{P}^k_{\min,\mu,\boldsymbol{\lambda}})$, the projection onto the constraint spaces is explicit. This allows the use of projected gradient methods to solve the minimization problems. Using a projected fixed-step gradient method on these dual problems is equivalent to using Uzawa algorithm [44] on the corresponding primal problems. The advantage of considering the dual problem is that we can take advantage of the many variants of the gradient algorithm. For example, Accelerated Projected Gradient Descent such as Nesterov algorithm are used in [28, 13] or various Krylov subspace and spectral methods in [16]. These accelerated algorithms still have a linear convergence rate, but they provide significant reductions in the number of iterations compared to the fixed-step gradient. A second strategy is to choose to solve the convex minimization problems using solvers than can deal with quadratic optimization under conic constraints and having a quadratic convergence rate. For example, the classical Primal-Dual Interior-Point was used in [37, 3, 20] to solve the minimization problem on forces and in [26] to solve the problem based on velocities. As expected, the number of iterations required to achieve a given accuracy is greatly reduced compared to gradient-like methods. However, each iteration is most costly and they can lose their competitive advantage compared to first order methods for large numbers of particles (see for example [29]). Improving the available algorithms to solve the friction problem is still an active domain of research. One can cite for example the recent works [10, 13] where the authors propose a method to accelerate the Newton step in second-order methods.

3.1.2 Gradient-like methods

Gradient-like methods are easy to implement and were proved in [29] to be efficient compared to classical, non accelerated, second order methods. In order to give the reader a complete vision of the techniques involved, we briefly describe here these algorithms and we illustrate their behavior through basic test cases. We refer to [28] for a deep investigation of accelerated projected gradient algorithms based on Nesterov algorithm.

Both force based problems, $(\mathcal{P}^k_{\min,\boldsymbol{\lambda}})$ (17) without friction and $(\mathcal{P}^k_{\min,\mu,\boldsymbol{\lambda}})$ (32) with friction, can be rewritten as:

$$\min_{\boldsymbol{\lambda}\in K} \ \frac{1}{2}\boldsymbol{\lambda}^T\mathbf{Q}\,\boldsymbol{\lambda} + \mathbf{C}^T\boldsymbol{\lambda},$$

where the projection Π_K on the set K is explicit.

The simplest algorithm for solving this problem is the fixed-step Projected Gradient Descent algorithm (PGD), corresponding to Uzawa's algorithm [44] for the associated primal problem (see Algorithm 1).

The gradient method can be accelerated using Nesterov's method [34] coupled to the projection step, and leading to an Accelerated Projected Gradient Descent algorithm (APGD) which is described in Algorithm 2.

As proposed in [28], Nesterov's algorithm can be augmented with adaptive step size. Indeed, the algorithm converges provided $\rho^{(n)} \leq 1/L$ where L is the Lipschitz constant of the cost function. We search for steps $\rho^{(n)}$ as large as possible and preserving the convergence. If the global constant L is not known in general, it can be estimated at each step n by a local constant $L^{(n)}$. For example, one can choose $\rho^{(n)} = 1/L^{(n)}$ and request that $L^{(n)}$ satisfies the following condition:

$$f(\boldsymbol{\lambda}^{(n+1)}) \leq f(\boldsymbol{\lambda}^{(n)}) + \nabla f(\mathbf{y}^{(n)})^T(\boldsymbol{\lambda}^{(n+1)} - \mathbf{y}^{(n)}) + \frac{L^{(n)}}{2}\left|\,\boldsymbol{\lambda}^{(n+1)} - \mathbf{y}^{(n)}\,\right|^2,$$

Algorithm 1 Fixed-step Projected Gradient Descent (PGD)

function GRADIENT($\mathbf{Q}$, $\mathbf{C}$, Π_K, ρ, tol)
  $n = 0$
  $\boldsymbol{\lambda}^{(0)} = 0$
  while $\frac{\left|\boldsymbol{\lambda}^{(n)} - \boldsymbol{\lambda}^{(n-1)}\right|}{\left|\boldsymbol{\lambda}^{(n-1)}\right| + 1} \leq \text{tol}$ **do**
    $\mathbf{dg}^{(n)} = \mathbf{Q}\boldsymbol{\lambda}^{(n)} + \mathbf{C}$
    $\boldsymbol{\lambda}^{(n+1)} = \Pi_K\left(\boldsymbol{\lambda}^{(n)} - \rho \mathbf{dg}^{(n)}\right)$
    $n = n + 1$
  return $\boldsymbol{\lambda}^{(n)}$
end function

Algorithm 2 Nesterov's Accelerated Projected Gradient Descent (APGD)

function ACCELERATED GRADIENT($\mathbf{Q}$, $\mathbf{C}$, Π_K, ρ, tol)
  $n = 0$
  $\boldsymbol{\lambda}^{(0)} = 0$
  $\mathbf{y}^{(0)} = 0$
  $\theta^{(0)} = 1$
  while $\frac{\left|\boldsymbol{\lambda}^{(n)} - \boldsymbol{\lambda}^{(n-1)}\right|}{\left|\boldsymbol{\lambda}^{(n-1)}\right| + 1} \leq \text{tol}$ **do**
    $\mathbf{dg}^{(n)} = \mathbf{Q}\mathbf{y}^{(n)} + \mathbf{C}$
    $\boldsymbol{\lambda}^{(n+1)} = \Pi_K\left(\mathbf{y}^{(n)} - \rho \mathbf{dg}^{(n)}\right)$
    $\theta^{(n+1)} = \frac{1}{2}\left(\theta^{(n)}\sqrt{4 + \left(\theta^{(n)}\right)^2} - \left(\theta^{(n)}\right)^2\right)$
    $\beta^{(n+1)} = \theta^{(n)}\frac{1 - \theta^{(n)}}{\left(\theta^{(n)}\right)^2 + \theta^{(n+1)}}$
    $\mathbf{y}^{(n+1)} = \boldsymbol{\lambda}^{(n+1)} + \beta^{(n+1)}\left(\boldsymbol{\lambda}^{(n+1)} - \boldsymbol{\lambda}^{(n)}\right)$
    $n = n + 1$
  return $\boldsymbol{\lambda}^{(n)}$
end function

where $f(\boldsymbol{\lambda}) = \frac{1}{2}\boldsymbol{\lambda}^T\mathbf{Q}\boldsymbol{\lambda} + \mathbf{C}^T\boldsymbol{\lambda}$ is the cost function. At each step, $L^{(n)}$ is first decreased ($L^{(n+1)} = 0.97L^{(n)}$ so that $\rho^{(n)}$ increase) and then increased ($L^{(n+1)} = 2L^{(n)}$) as long as the previous condition is violated (see [28] for more details). This leads to an Accelerated Projected Gradient Descent algorithm with Adaptive Step denoted by APGD-AS in the following. Again following [28], an adaptive restart can be implemented by setting $\theta^{(n+1)} = 1$ whenever $\nabla f(\mathbf{y}^{(n)})^T(\boldsymbol{\lambda}^{(n+1)} - \boldsymbol{\lambda}^{(n)}) > 0$. This leads to an algorithm denoted by APGD-AR in the following. The algorithm implementing both adaptive step and restart is denoted by APGD-ASR.

To compare the behavior of the different gradient algorithms, we consider the following configuration: a disk with radius $r = 1$ and mass $m = 1$ is placed on an inclined plane with angle $\alpha = \pi/6$, and the gravity is set to $\mathbf{g} = (0, -1)$ (see Figure 15). It's initial velocity is set to zero.

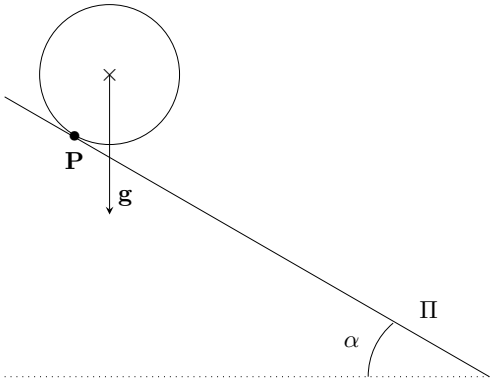

Figure 3: Notations. Disk placed on an inclined plane.

The time-step is $\Delta t = 0.05$ and we compute the solution to the first time-step optimization problem in the non frictional case. For each solver, the tolerance is set to tol $= 10^{-9}$ and the step (initial step in case of an adaptive step algorithm) is $\rho = 2$. We plot on Figure 4 the evolution of the constraint and the cost function as a function of the iterations. The convergence of PDG algorithm is monotonous and, as expected, the accelerated algorithms converge quicker.

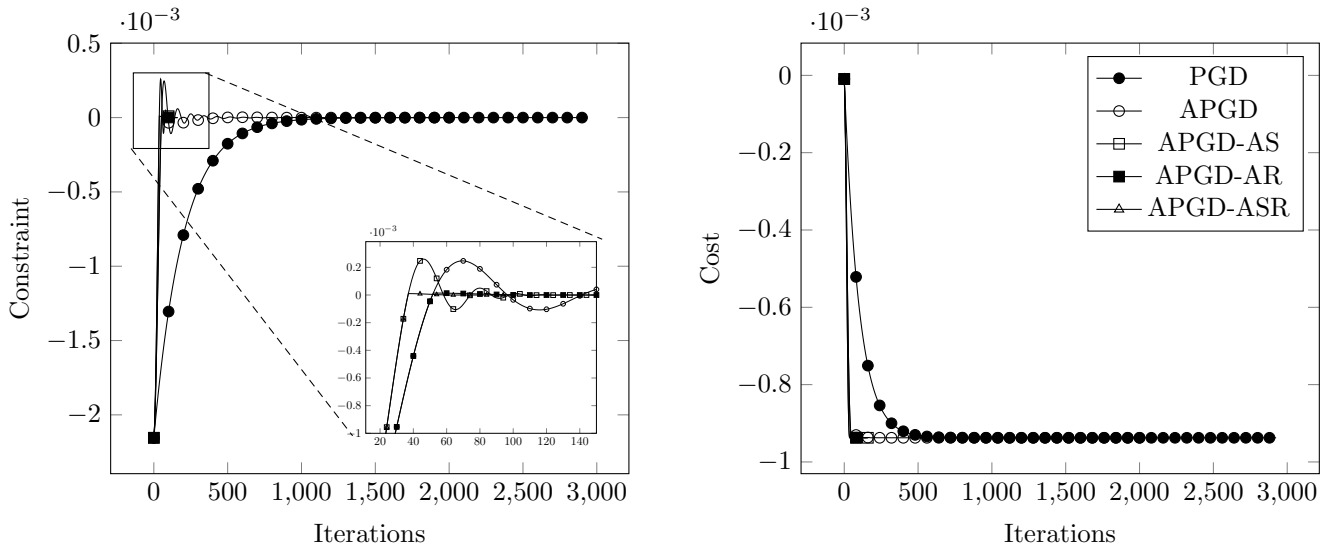

Figure 4: Disk placed on a plane without friction. Evolution of the constraint (left) and cost (right) as a function of the iterations for the different gradient minimization algorithms implemented in SCoPI.

The corresponding number of iterations required for each algorithm to reach accuracies of 10^{-3} and 10^{-9} are given in Table 1.

Solver	Number of iterations tol $= 10^{-3}$	Number of iterations tol $= 10^{-9}$
PGD	206	2926
APGD	68	2029
APGD-AS	47	164
APGD-AR	54	160
APGD-ASR	39	100

Table 1: Disk placed on a plane without friction. Number of iterations as a function of solver and tolerance

3.2 Convergence of the numerical schemes

In this section, the inner solver is fixed and we focus on the convergence of the different schemes when the time-step Δt goes to zero. As already said, very few theoretical results can be found in the litterature and the demonstrations are based on compactness methods. No study (theoretical or numerical) of the convergence speed is available. To illustrate the good behavior of the different schemes, we consider in the following the same configuration as in the previous section, the disk being now initially located above the plane (at distance r). We have an explicit solution to the problem with and without friction (see appendix B), which allows us to study numerically the convergence of the numerical solutions when the time-step vanishes.

3.2.1 Disk falling on a plane without friction.

We plot on Figure 5 the numerical solution based on the convex problems ($\mathcal{P}^k_{\text{min},\boldsymbol{\lambda}}$) and computed with the code SCoPI for $\Delta t = 0.05$, using the APGD-ASR algorithm with parameters $\rho = 2$ and tol $= 10^{-9}$ to solve the inner incremental problem. The exact solution is plotted on the same figure. We place ourselves in the reference frame adapted to the plane: normal and tangential directions to the plane. In a first stage, the disk falls with a constant acceleration (linear velocity) and then touches the plane. After the instant of contact, the normal velocity is zero (the disk remains on the plane) and, as there is no frictional force, the tangential velocity continues to grow linearly with the same slope.

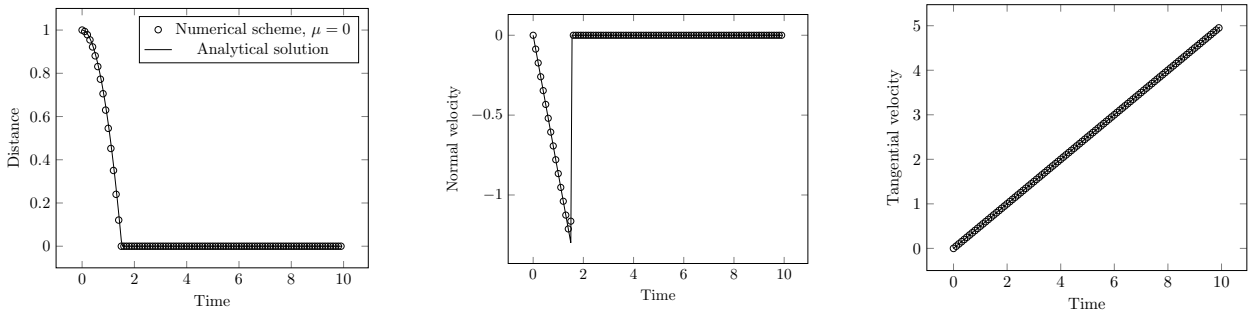

(a) Distance (b) Normal velocity (c) Tangential velocity

Figure 5: Disk falling on a plane without friction. Distance (left plot), normal velocity (middle plot), and tangential velocity (right plot). Solution obtained with the code SCoPI and analytical solution.

The L^2 error between the numerical and exact solutions is defined as

$$e_{\Delta t,\mathbf{x}} = \sqrt{\sum_k \Delta t \,|\, \mathbf{x}(t^k) - \mathbf{x}^k \,|^2}, \quad e_{\Delta t,\theta} = \sqrt{\sum_k \Delta t (\theta(t^k) - \theta^k)^2},$$

where $t \mapsto (\mathbf{x}(t), \theta(t)) \in \mathbb{R}^3$ is the exact position of the center and angular orientation and $(\mathbf{x}^k, \theta^k) \in \mathbb{R}^3$ the corresponding numerical approximation at k-th time-step t^k. Without friction, the sphere does not roll on the plane so that only $e_{\Delta t,\mathbf{x}}$ is relevant. We can see from Figure 6 that the numerical scheme converges with order 1 for this test.

3.2.2 Disk falling on a plane with friction.

We now consider the same numerical experiment as in the previous section, with frictional contact. In that case, we have two schemes at hand to compute a numerical approximation at time-step k: the convexified

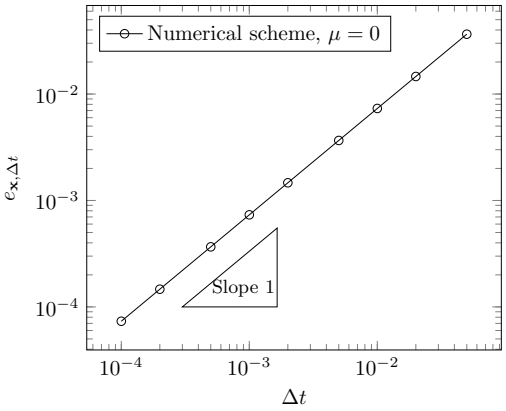

Figure 6: Disk falling on a plane without friction. L^2 error on the position of the center of the disk as a function of Δt.

scheme ($\mathcal{P}^k_{\min,\mu,\boldsymbol{\lambda}}$) and the fixed point method ($\mathcal{P}^k_{\mathrm{FP},\mu,\boldsymbol{\lambda}}$). We plot on Figure 7 the exact solution, together with the two corresponding numerical approximations. The numerical solutions are computed for $\Delta t = 0.05$ and the inner problems (based on a conic constraint) are solved using `Mosek` solver with default parameters [33]. The stopping criterion for the fixed-point problem is $(s^{p+1} - s^p)/(s^p + 1) \leq \mathrm{tolFP}$ where $\mathrm{tolFP} = 10^{-2}$. The test is run for two values of the friction coefficient: $\mu = 1$ (rolling motion) and $\mu = 0.1$ (slipping motion). At a first stage, until contact, the disk falls with constant acceleration, without rotation. By touching the plane, the translation and angular velocities are instantaneously modified by the contact law: the normal velocity vanishes and the tangential and angular velocities undergo a shock. Then, the normal velocity remains zero (the disk remains on the plane) and the tangential and angular velocities becomes linear again, with a slope modified by the friction force.

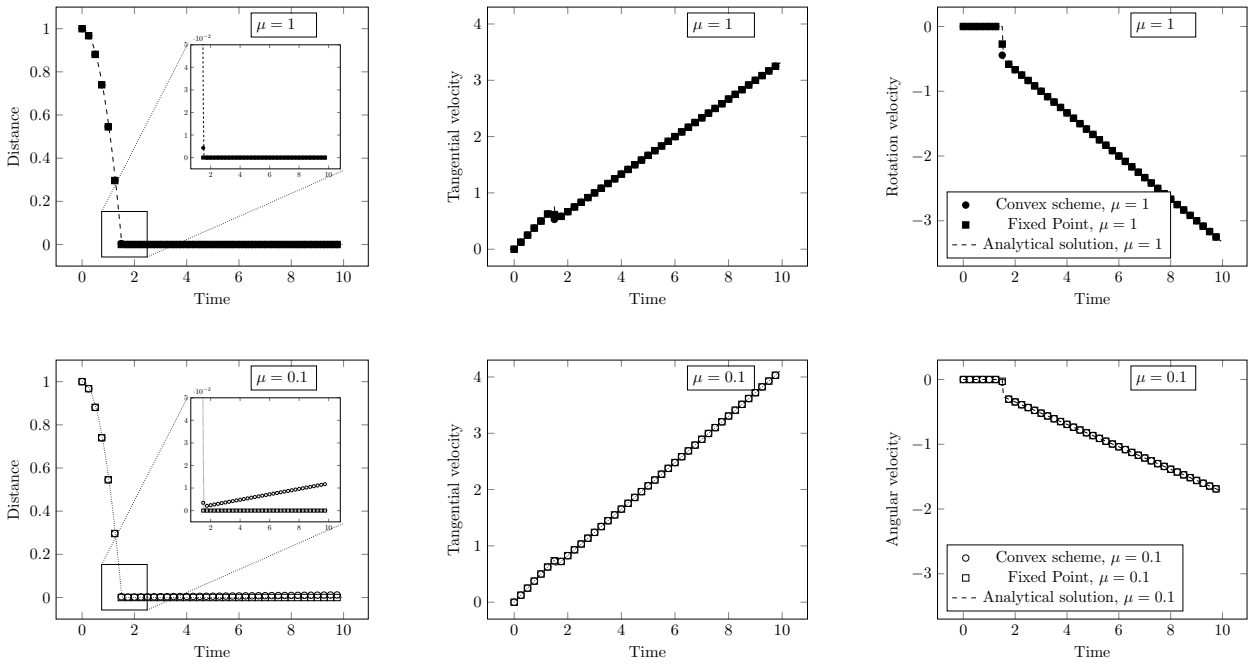

(a) Distance (b) Tangential velocity (c) Angular velocity

Figure 7: Disk falling on a plane with friction. Distance (left), tangential velocity (center), and rotation velocity (right), for $\mu = 1$ (top panels, rolling motion) and $\mu = 0.1$ (bottom panels, slipping motion). Solutions obtained with the code SCoPI and analytical solution.

Although the numerical solutions computed by the two schemes have the same behavior, one can observe the effect of convexification on the insets of the left column. In the case of the fixed point algorithm (square

marks), after convergence, we have $F(s^\star) = s^\star$ (see equation (40)) so that the final constraint is

$$\mathbf{D}_n^k + \Delta t\, N_\alpha^k A_\alpha^k \mathbf{u}^{k+1} \geq \mu \Delta t (F(s^\star)_\alpha - s_\alpha^\star) = 0\,,\ \alpha \in I_c,$$

and the distance is equal to zero after contact. The situation is different when solving the convexified problem (circle marks). First of all, in the case of a rolling motion ($\mu = 1$, Figure 7(A) – top panel), the relative velocity of the contact point is zero so that the constraint verified by the numerical solution is again

$$\mathbf{D}_n^k + \Delta t\, N_\alpha^k A_\alpha^k \mathbf{u}^{k+1} \geq \mu \Delta t \left| T_\alpha^k A_\alpha^k \mathbf{u}^{k+1} \right| = 0\,,\ \alpha \in I_c.$$

Consequently, in the case of a rolling motion, the convex problem leads to null distances after contact. But in the case of a sliding motion, the relative speed is not zero (and even increases linearly during the motion) so that we have

$$\mathbf{D}_n^k + \Delta t\, N_\alpha^k A_\alpha^k \mathbf{u}^{k+1} \geq \mu \Delta t \left| T_\alpha^k A_\alpha^k \mathbf{u}^{k+1} \right| > 0\,,\ \alpha \in I_c.$$

In that case, the distance during contact is positive and some numerical dilatation occurs ($\mu = 0.1$, see inset Figure 7(A) – bottom panel). Note that, although the corresponding dilatation is controlled by the time-step Δt, the error due to the discretization of the constraint is now of order Δt at each time-step. This could theoretically affect the convergence of the convexified scheme. On its side, the fixed point method recovers the original Taylor expansion, only introducing an error of order Δt^2 at each time-step. In order to check the good behavior of the two algorithms, we plot on Figure 8 the corresponding L^2 error for both methods. To observe the error of the scheme and not the one resulting from the incremental problem resolution, `Mosek` accuracy parameters are set to 10^{-11} for this test. We can see that both algorithms actually converge to the exact solution with order 1 in Δt. Finally, let us note that the fixed point algorithm, contrary to the convexified problem, is based on an iterative method and thus solves several optimization problems for each iteration in time. For this test case, the average number of iterations is independent of the time-step and it performs on average 2.8 iterations for $\mu = 1$ and 1.2 iterations for $\mu = 0.1$.

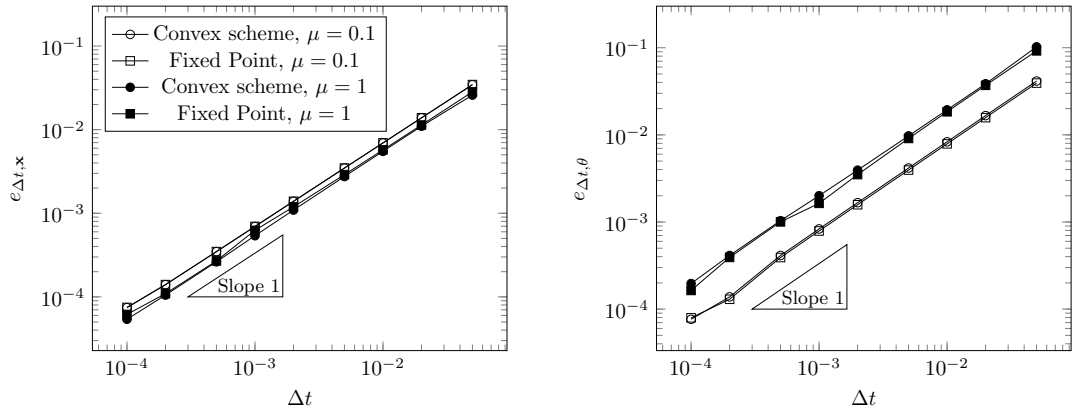

(a) Error on the position

(b) Error on the rotation angle

Figure 8: Disk falling on a plane with friction. L^2 error on the position of the center of the disk (left pannel) and the rotation angle (right pannel) as a function of Δt, with different solvers and different values of μ.

3.3 Multiparticle tests

In this section we first confirm, following [28], the good behavior of the gradient-like methods when the number of particles increase. Then, in case of frictional contacts, the convexified and fixed point schemes are compared. In particular, we study the influence of the constraint convexification on the macroscopic behavior of the system.

3.3.1 Frictionless model. Behavior of the gradient-like methods when the number of particles increases.

As shown in [28], we check here that the accelerated gradients algorithms behave well when the number of particles increase.

At each time-step, the CPU time required to compute the solution to the optimization problem depends strongly on the number of constraints imposed. Although all constraints $\alpha \in I_c$ must be verified, it is obvious that those related to very distant pairs of particle will not be activated (the contact force will be zero). In order to optimize the computation time, we therefore consider in the sets of constraints K only the *neighboring particles*, whose distance is below a given threshold D_{max}: $\alpha \in \bar{I}_c = \{\alpha,\, D_\alpha \geq D_{max}\}$. Among these pairs of neighboring particles, some will come into contact during the considered time-step, and others not. We call *active contacts* the pairs of particles in contact (i.e. for which the Lagrange multiplier, or equivalently the contact force, is not zero). In the following, given that the maximum displacement of a particle during a time-step is 20% of its radius, we set D_{max} to the largest value of the radii of the particles.

We consider $N = n^3$ particles whose centers are initially placed on a regular grid in a cubic box of side $L = 10$. If $\delta = L/n$ is the step-size of the corresponding grid, the radii of the spheres are generated according to a uniform law in $[0.8\,\delta/2,\, 0.9\,\delta/2]$. In order to obtain an initial configuration in which the spheres are not aligned, a random displacement uniformly generated in $[-0.05\,\delta/2,\, 0.05\,\delta/2]$ is added to the centers of the spheres (see Figure 9(left) for $N = 125\,000$ particles). The mass is uniformly chosen in $[1, 2]$ and the gravity is $g = -1$. The time-step is chosen so that the particles do not move more than 20% of their radius per time iteration. The parameters of the different solvers are set to $\rho = 0.2/\Delta t^2$ and $\mathrm{tol} = 10^{-3}$. The stationary state obtained for $t = 8$ with algorithm APGD-AR is plotted on Figure 9(right).

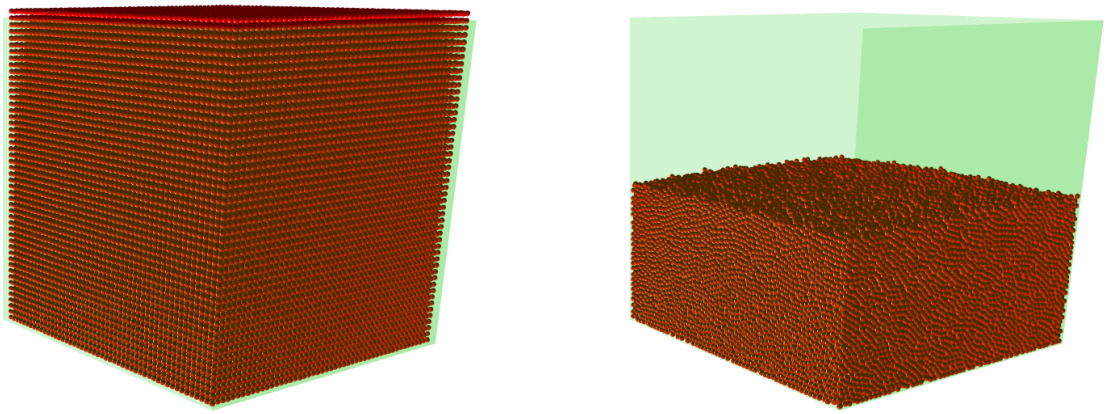

Figure 9: 125 000 particles falling in a box without friction. Initial configuration (left) and stationary state computed with algorithm APGD-AR (right)

We compare on Figure 10 the number of iterations of the different solvers as a function of the number of active contacts for the simulation with 125 000 particles. We observe that, as expected, PGD performs more iterations than the accelerated gradient methods. Even though APGD-ASR is the algorithm performing the least number of iterations, the different accelerated versions have a similar behavior, linear in the number of contacts.

We compare in Table 2 the computation time of the different algorithms. The second to last columns illustrates the behavior of each algorithm when the number of particles increase. For each algorithm, we give the computational time for 125 000 particles, normalized by the time spent by the same algorithm for 512 particles. We can see that, for, about 250 more particles, 400 more constraints and 220 more active contacts, the different algorithms spent about 13 times more time to compute the solutions. We also indicate in the last column, the gain in terms of computational time of the different accelerated algorithms, compared to PGD for the same number of particles. We observe that, although APGD-ASR performs fewer iterations, the corresponding computation time is higher than that of APGD-AR, the search for the optimal step being expensive.

3.3.2 Frictional model. Comparison of the convexified and the fixed point schemes.

In the following, we now compare the behavior, for increasing numbers of particles, of the two schemes that approximates the frictional problem: the convexified scheme ($\mathcal{P}^k_{\min,\mu,\boldsymbol{\lambda}}$) and the fixed point method ($\mathcal{P}^k_{\mathrm{FP},\mu,\boldsymbol{\lambda}}$).

Since each iteration of the fixed point method consists in solving a convexified problem, the comparison of the computation times of the two algorithms essentially amounts to a comparison of the number of iterations

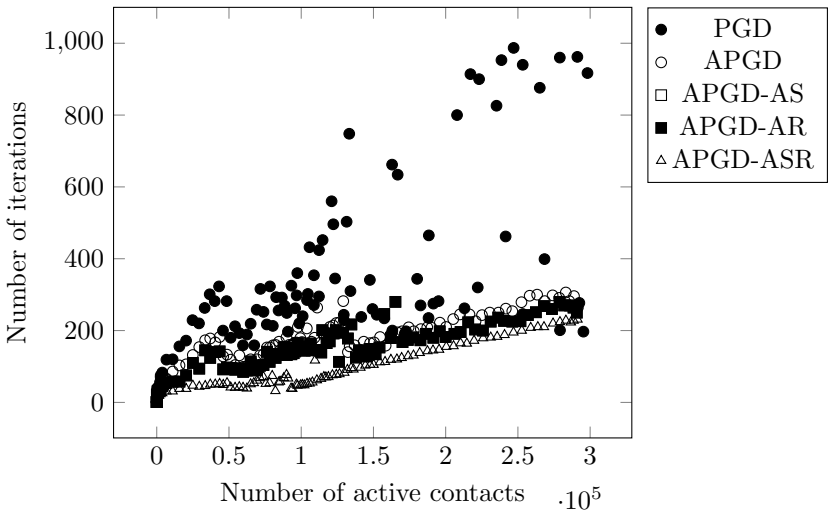

Figure 10: 125 000 particles falling in a box without friction. Number of iterations of the different solvers as a function of the number of active contacts.

Solver	Number of particles (N)	Final number of constraints	Final number of active contacts	Computation time – influence of N –	Computation time – acceleration –
PGD	512	2 426	1 488	–	–
APGD	512	2 439	1 354	–	0.37
APGD-AS	512	2 452	1 416	–	0.66
APGD-AR	512	2 418	1 372	–	0.31
APGD-ASR	512	2 428	1 447	–	0.45
PGD	125 000	910 646	299 758	9.4	–
APGD	125 000	910 867	292 170	12.9	0.51
APGD-AS	125 000	910 794	291 796	14.4	1.01
APGD-AR	125 000	910 715	292 480	12.9	0.43
APGD-ASR	125 000	910 238	292 839	14.2	0.69

Table 2: Falling particles without friction. Number of contacts, number of iterations, and computational time as a function of the different solvers and as a function of the number of particles.

of the fixed point. To achieve this comparison, we consider a group of particles arranged in a (fictitious) cube as in the previous test case and now falling on a horizontal plane. We plot Figure 11 the initial configuration, as well as the configuration obtained at time $t = 2.58$ with $\Delta t = 0.0086$, $N = 1\,728$ and $\mu = 1$ for the fixed point algorithm. The planes drawn on the figures are fictitious planes: they are not taken into account in the simulation but allow to visually compare the two figures (spreading, height of the pile of particles). We

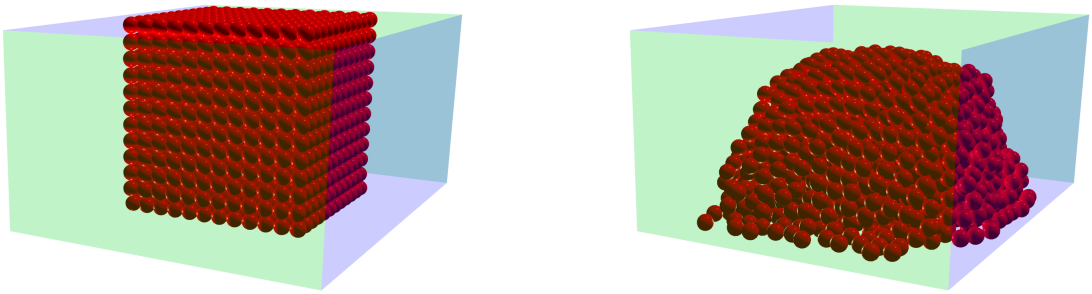

Figure 11: 1 728 particles falling on an horizontal plane with friction. Initial configuration (left) and configuration at $t = 2.58$ (right) for $\mu = 1$. Fixed point algorithm.

ran the simulations for $N = 512$, $N = 1000$ and $N = 1728$. As observed in [2], the number of iterations of the fixed point does not depend much on the number of particles. It depends on the friction coefficient: in our test cases, we observe on average 3.5 iterations for $\mu = 0.1$ and 8 iterations for $\mu = 1$.

In parallel to the comparison of the computation time, it is interesting to measure the effect of the constraint convexification on the macroscopic behavior observed during the simulations. Indeed, as we have already pointed out, if the convexified scheme is obviously faster, it causes a numerical dilation effect in the granular medium (see Section 3.2.2). A comparison has been made in [26] showing that, on a 2d column collapse problem, the profiles obtained with the convexified scheme, as well as the dynamics, were comparable to those previously obtained by the NSCD method solving the non-convex LCP problem. Here, we compare the convexified and the fixed point schemes on the collapse of $30^2 = 900$ disks, falling on a horizontal plane in 2d. The disks are initially placed on a regular grid of width and height $H = 10$. All the spheres have the same radius $r = H/(2 \times 31)$ and have a random mass between 1 and 2. In order to break the symmetry, the first row is shifted by $r/2$. The gravity is set to -1. The time-step is chosen so that the spheres move at most 10% of their radius. We compare on Figure 12 the profiles computed at different times, for friction coefficients $\mu = 0.1$ and $\mu = 1$. One can see that the profiles and dynamics obtained using the two schemes are similar.

3.3.3 Non-spherical particles

Finally, let us illustrate how the different schemes can be used for non-spherical particles. The additional difficulty in this case is the computation of the points realizing the minimal distance between the particles. Indeed, contrary to the case of spheres, we do not have any analytical expression for these points, even for simple non-spherical shapes such as ellipses in 2d. It is well known that this calculation is of critical importance in DEM simulations of granular media at the grain scale, and that it takes time. One can for example cite [24, 23, 35, 45, 8], in which different algorithms are proposed to solve this problem. In our simulations, we choose to solve a nonlinear system by a Newton-type method, in order to find the common normals of the two particles at these minimal distance points.

The method is tested in 2d without friction by considering a column collapse of 100 ellipses. The major axis of each ellipses in the vertical direction is $r = 0.45$ and is chosen randomly between 0.22 and 0.68 in the horizontal direction (see initial configuration on Figure 13(A)). The gravity is set to 5 and the mass is randomized between 1 and 2. The plane is composed of small glued spheres of radius 0.045. The solver is APGD-AR with $\text{tol} = 10^{-3}$ and $\Delta t = 0.01$. The configurations obtained are given for different time-steps on Figure 13.

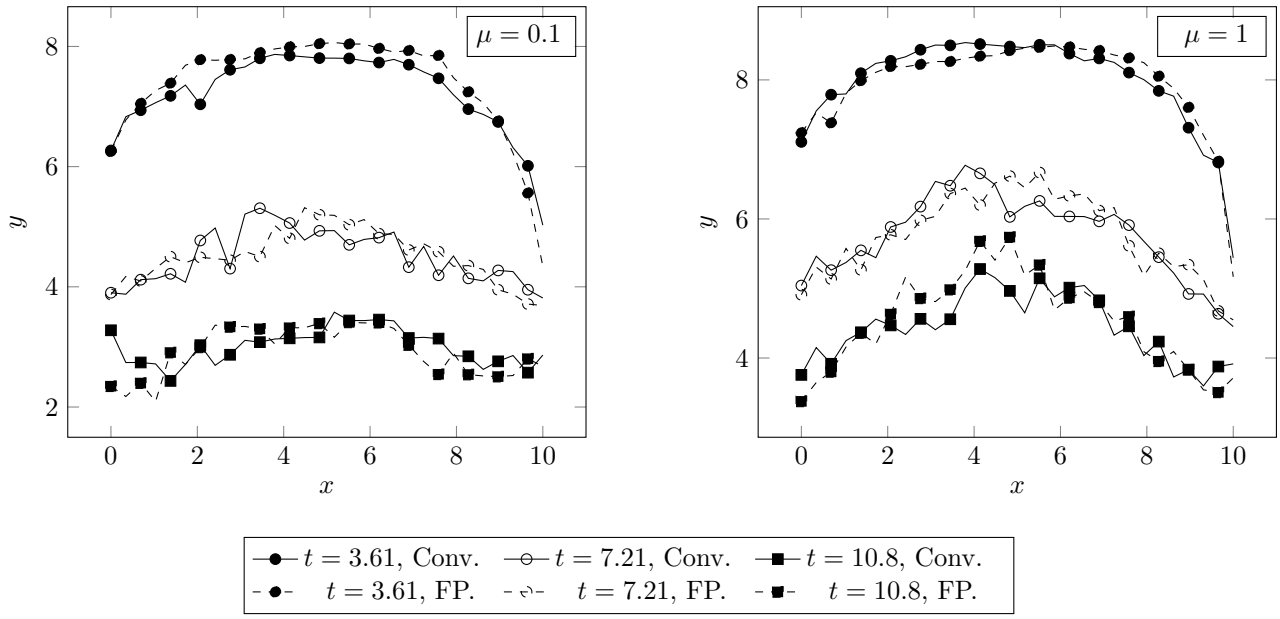

Figure 12: 2d column collapse with friction. Comparison of the profiles obtained at different times by the convexified scheme (Conv. – dashed lines) and the fixed point scheme (FP. – plain lines). $\mu = 0.1$ (left panel) and $\mu = 1$ (right panel).

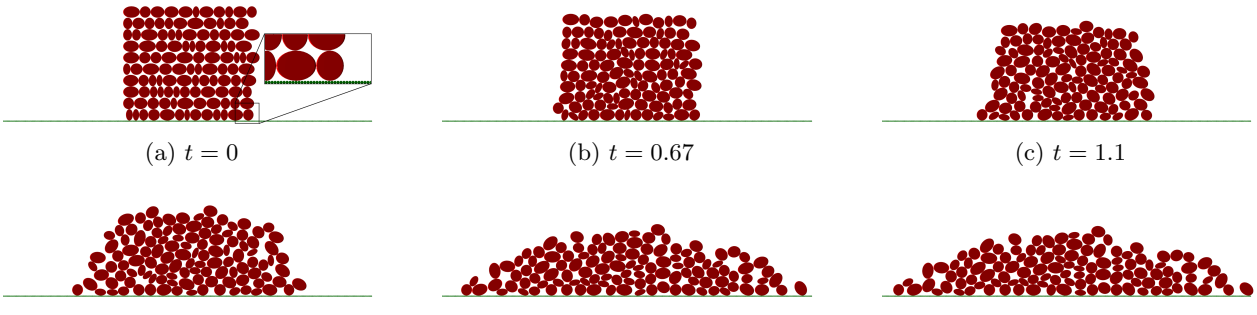

(a) $t = 0$ (b) $t = 0.67$ (c) $t = 1.1$

(d) $t = 2.6$ (e) $t = 2.4$ (f) $t = 2.5$

Figure 13: 2d column collapse of ellipses without friction. Snapshots at different times.

4 Conclusion

This paper is a self-contained review of existing schemes based on convex discrete incremental problems, for simulating granular media. These schemes can be seen as convex minimization problems for which the optimality conditions result in a formal discretization of the fundamental principle of dynamics: the local contact laws are satisfied. We have shown that they can also be understood as the minimization of a global discrete energy problem for the whole system, in which the velocity to be considered is an average of the pre- and post-impact velocities, as suggested by Frémond in [15]. No theoretical or numerical results concerning the convergence speed of the schemes we consider are available. We have conducted a numerical study showing that each of them converges with order one in the time step (for an academic test case whose solution is known). We also showed that, on a 2d column collapse test case, the convex constraint relaxation, although inducing a numerical dilatation, does not significantly modify the macroscopic behavior of the medium. The numerical tests have been performed with the code SCoPI developed at the CMAP laboratory and the behavior of the different algorithms for large numbers of particles is very encouraging. A future work will consist in coupling these contact schemes with fluid/particle solvers and with the gluey particle scheme proposed in [21]. The latter has been developed to take into account lubrication in simulations of suspensions and falls within the same convex optimization framework as the schemes described in this paper. This will provide a numerical tool taking into account both friction and lubrication and based on a stable Contact Dynamics scheme.

A Notion of sub-differential.

In this appendix, some definitions and results on subdifferentials are given, useful for understanding the model with friction. The notion of subdifferential allows to describe the local variations of a convex function, not necessarily derivable. We refer to [17, Chap. VI] for an extensive description of subdifferentials and their use in optimisation.

A.1 Definition.

Let us consider a convex function $\phi : \mathbb{R}^n \to \mathbb{R}$. The subdifferential of ϕ at point $\mathbf{x} \in \mathbb{R}^n$, denoted by $\partial\phi[\mathbf{x}]$, can be defined through minorization by affine functions:

$$\partial\phi[\mathbf{x}] = \{\mathbf{y} \in \mathbb{R}^n / \quad \forall \hat{\mathbf{x}} \in \mathbb{R}^n, \quad \phi(\hat{\mathbf{x}}) \geq \phi(\mathbf{x}) + \mathbf{y} \cdot (\hat{\mathbf{x}} - \mathbf{x})\}\,.$$

Let us illustrate this notion in one dimension (see Figure 14). In that case, the subdifferiential contains the slopes of the lines issued from point $(\mathbf{x}, \phi(\mathbf{x}))$ and remaining under the graph. If ϕ is derivable at point x_0, we have $\partial\phi[x_0] = \{\phi'(x_0)\}$. More generally, if ϕ is left and right derivable at point x_1, $\partial\phi[x_1]$ is a closed interval: $\partial\phi[x_1] = [\phi'(x_1{}^-), \phi'(x_1{}^+)]$.

Figure 14: Subdifferential. Left: the function is differentiable at point x_0. Right: the function is not differentiable at point x_1.

For example, if $\mathrm{abs} : \mathbb{R} \to \mathbb{R}$ is the absolute value, $\mathrm{abs}(x) = |x|$, then

$$\partial\,\mathrm{abs}[x] \underset{x>0}{=} \{1\}, \quad \partial\,\mathrm{abs}[x] \underset{x<0}{=} \{-1\}, \quad \text{and} \quad \partial\,\mathrm{abs}[0] = [-1, 1].$$

Note that, whatever is the dimension, a function $\phi : \mathbb{R}^n \to \mathbb{R}$ is differentiable at $\mathbf{x}_0$ if and only if the set $\partial\phi[\mathbf{x}_0]$ contains only one point. In that case, this point is the gradient of ϕ at $\mathbf{x}_0$. Then we have:

$$\phi \text{ differentiable at } \mathbf{x}_0 \Longrightarrow \partial\phi[\mathbf{x}_0] = \{\nabla\phi(\mathbf{x}_0)\}\,.$$

A.2 Optimality conditions and Lagrange multipliers for non-differentiable functions.

The notion of subdifferential allows to generalize optimality conditions for non-differentiable functions. Indeed, as illustrated by the red dashed slope on Figure 14, if ϕ is convex we have

$$\mathbf{x} \text{ is a minimum of } \phi \Longleftrightarrow 0 \in \partial\phi[\mathbf{x}].$$

In case ϕ is differentiable, this equivalence is the usual optimality condition for convex functions: $\mathbf{x}$ is a minimum of ϕ if and only if $\nabla\phi(\mathbf{x}) = 0$.

Another generalization of optimality condition, used in (29), is the generalization to a non-differentiable constraint of the Kuhn-Tucker optimality condition. Let us consider the minimization problem

$$\min_{\mathbf{x}\in K} J(\mathbf{x}), \quad K = \{\mathbf{x} \in \mathbb{R}^n,\ g(\mathbf{x}) \leq 0\},$$

where $J : \mathbb{R}^n \to \mathbb{R}$ is a differentiable convex function and $g : \mathbb{R}^n \to \mathbb{R}$ is convex. Then, if the constraint at point $\mathbf{x}$ is *qualified* (see below), $\mathbf{x}$ is a minimum of J on K if and only if there exists a Lagrange multiplier λ such that the following Kuhn-Tucker optimality condition is verified [17, Thm. 2.1.4 p. 305]:

$$\begin{aligned} &\nabla J(\mathbf{x}) \in -\lambda\, \partial g[\mathbf{x}], \\ &g(\mathbf{x}) \leq 0, \quad \lambda \geq 0, \quad g(\mathbf{x})\lambda = 0. \end{aligned} \tag{41}$$

As for the differentiable case, the qualification of the constraint is needed to prove the existence of the Lagrange multipliers when $\mathbf{x}$ is a minimum (it is not necessary for the reverse implication, which follows from the convexity assumptions). For the frictional problem (29), we use the Slater qualification assumption saying that, if g is not affine, it is sufficient to check that there exists a point $\mathbf{x}_0$ in K for which the constraint is strictly satisfied:

$$\exists \mathbf{x}_0 \in K \text{ such that } g(\mathbf{x}_0) < 0 \quad \text{(Slater qualification condition)}. \tag{42}$$

A.3 A useful example.

We consider in the following an example we use to compute the sub-differentials of the constraints $g^k_{\alpha,\mu}$ in (28). We denote by P the projection onto a plane Π in dimension 3 and consider the following function

$$\begin{aligned} h : \mathbb{R}^3 &\to \mathbb{R} \\ \mathbf{v} &\to |P\mathbf{v}|. \end{aligned}$$

Let us prove that

$$|P\mathbf{v}| \neq 0 \Longrightarrow \partial h[\mathbf{v}] = \left\{ \frac{P\mathbf{v}}{|P\mathbf{v}|} \right\}, \tag{43}$$

$$|P\mathbf{v}| = 0 \Longrightarrow \partial h[\mathbf{v}] = \left\{ \mathbf{w} \in \mathbb{R}^3 \text{ s.t. } \mathbf{w} \in \Pi \text{ and } |\mathbf{w}| \leq 1 \right\}. \tag{44}$$

- In case $|P\mathbf{v}| \neq 0$, h is differentiable so that $\partial h[\mathbf{v}] = \{\nabla h(\mathbf{v})\}$. To compute the gradient of h, we simply write, using a Taylor expansion,

  $$h(\mathbf{v} + \epsilon\mathbf{w}) = |P(\mathbf{v} + \epsilon\mathbf{w})| = |P\mathbf{v} + \epsilon P\mathbf{w}| = h(\mathbf{v}) + \epsilon \frac{P\mathbf{v}}{|P\mathbf{v}|} \cdot P\mathbf{w} + o(\epsilon^2).$$

  It remains to remark that, since $P\mathbf{w} - \mathbf{w} \perp \Pi$ and $P\mathbf{v} \in \Pi$, we have $\dfrac{P\mathbf{v}}{|P\mathbf{v}|} \cdot P\mathbf{w} = \dfrac{P\mathbf{v}}{|P\mathbf{v}|} \cdot \mathbf{w}$ so that

  $$h(\mathbf{v} + \epsilon\mathbf{w}) = h(\mathbf{v}) + \epsilon \frac{P\mathbf{v}}{|P\mathbf{v}|} \cdot \mathbf{w} + o(\epsilon^2).$$

  which concludes the proof of (43).

- In case $|P\mathbf{v}| = 0$, h is no more differentiable at point $\mathbf{v}$. Let us first prove that

  $$\partial h[\mathbf{v}] \subset \left\{ \mathbf{w} \in \mathbb{R}^3 \text{ s.t. } \mathbf{w} \in \Pi \text{ and } |\mathbf{w}| \leq 1 \right\}.$$

So let $\mathbf{w} \in \partial h[\mathbf{v}]$. First, we have $\mathbf{w} \in \Pi$. Indeed, if $\mathbf{n}$ is the normal to Π, we consider $\hat{\mathbf{v}}_\lambda = \mathbf{v} + \lambda\mathbf{n}$. Since $\mathbf{n} \perp \Pi$, $h(\hat{\mathbf{v}}_\lambda) = |P(\mathbf{v} + \lambda\mathbf{n})| = |P(\mathbf{v})| = h(\mathbf{v})$. Then, from $\mathbf{w} \in \partial h[\mathbf{v}]$, we obtain

$$\forall \lambda \in \mathbb{R}, \quad h(\mathbf{v}) = h(\hat{\mathbf{v}}_\lambda) \geq h(\mathbf{v}) + \mathbf{w} \cdot (\hat{\mathbf{v}}_\lambda - \mathbf{v}) = h(\mathbf{v}) + \lambda \mathbf{w} \cdot \mathbf{n},$$

and this cannot be true for any $\lambda \in \mathbb{R}$ unless $\mathbf{w} \cdot \mathbf{n} = 0$ i.e. $\mathbf{w} \in \Pi$.
Let us now prove that $|\mathbf{w}| \leq 1$. To do so, we consider $\hat{\mathbf{v}} = \mathbf{v} + \mathbf{w}$. Using on the one hand that $P\mathbf{v} = 0$ and on the other hand that $P\mathbf{w} = \mathbf{w}$ (since $\mathbf{w} \in \Pi$), we obtain

$$|\mathbf{w}| = |P(\mathbf{v} + \mathbf{w})| = h(\hat{\mathbf{v}}) \geq h(\mathbf{v}) + \mathbf{w} \cdot (\hat{\mathbf{v}} - \mathbf{v}) = \mathbf{w} \cdot (\hat{\mathbf{v}} - \mathbf{v}) = |\mathbf{w}|^2,$$

so that $|\mathbf{w}| \leq 1$ as expected.

- In now remains to prove the reverse inclusion when $|P\mathbf{v}| = 0$. Suppose that $\mathbf{w} \in \Pi$ and $|\mathbf{w}| \leq 1$. In that case, for all $\hat{\mathbf{v}} \in \mathbb{R}^3$ we have

$$h(\mathbf{v}) + \mathbf{w} \cdot (\hat{\mathbf{v}} - \mathbf{v}) \underset{P\mathbf{v}=0}{=} \mathbf{w} \cdot (\hat{\mathbf{v}} - \mathbf{v}) \underset{\mathbf{w}\in\Pi}{=} \mathbf{w} \cdot (P\hat{\mathbf{v}} - P\mathbf{v}) \underset{P\mathbf{v}=0}{=} \mathbf{w} \cdot P\hat{\mathbf{v}} \underset{|\mathbf{w}|\leq 1}{\leq} |P\hat{\mathbf{v}}| = h(\hat{\mathbf{v}}),$$

which proves that $\mathbf{w} \in \partial h[\mathbf{v}]$.

To finish with the computations of subdifferentials, let us consider

$$h_A : \mathbb{R}^n \to \mathbb{R}, \quad h_A(\mathbf{u}) = h(A\mathbf{u}) = |PA\mathbf{u}|,$$

where $A : \mathbb{R}^n \to \mathbb{R}^3$ linear. The rule for pre-composition with a linear mapping [17, Thm. 4.2.1 p. 263] gives $\partial h_A(\mathbf{u}) = A^T \partial h(A\mathbf{u})$ so that

$$\begin{aligned} |PA\mathbf{u}| \neq 0 &\Longrightarrow \partial h_A[\mathbf{u}] = \left\{ A^T \frac{PA\mathbf{u}}{|PA\mathbf{u}|} \right\}, \\ |PA\mathbf{u}| = 0 &\Longrightarrow \partial h_A[\mathbf{u}] = \left\{ A^T\mathbf{w}, \mathbf{w} \in \mathbb{R}^3 \text{ s.t. } \mathbf{w} \in \Pi \text{ and } |\mathbf{w}| \leq 1 \right\}. \end{aligned} \tag{45}$$

B A disk falling on an inclined plane: explicit solution.

In this appendix, we compute the explicit solutions used in section 3 to study the convergence of the different schemes. We consider a disk falling on an inclined plane, with and without friction.

B.1 Notations

We consider in 2d a line (called "plane" in the following) passing through the point (0,0) and inclined with an angle α from the horizontal. A disk of center $\mathbf{c}$, mass m, radius R and moment of inertia $J = \frac{m}{2}R^2$ is falling on the plane (see Figure 15). The equations of motion are written in the reference frame of the plane: $\mathbf{n}$ is the normal to the plane and $\mathbf{t}$ the tangent direction. Any vector $\mathbf{x} \in \mathbb{R}^2$ is decomposed in a normal and a tangential part:

$$\mathbf{x} = x_n\mathbf{n} + x_T\mathbf{t}.$$

At $t = 0$, the disk is placed at a distance h from the plane with a zero initial velocity:

$$\mathbf{c}(0) = (h + R)\mathbf{n}, \quad \mathbf{v}(0) = 0.$$

The velocity of the center of the disk is denoted by $\mathbf{v} = v_n\mathbf{n} + v_T\mathbf{t}$ and its angular velocity is ω. Its motion is decomposed into three parts: the free fall, the impact with the plane and the motion on the plane.

B.2 Free fall

During the free fall, the disk is only subject to the gravity $\mathbf{g}$. The equations of motion of its center write,

$$\begin{aligned} m\frac{dv_T}{dt} &= mg\sin\alpha, \\ m\frac{dv_n}{dt} &= -mg\cos\alpha, \\ J\frac{d\omega}{dt} &= 0. \end{aligned}$$

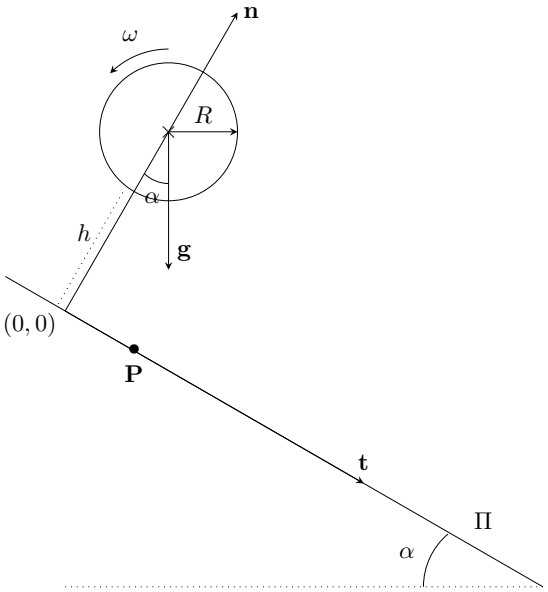

Figure 15: Notations. Disk falling on an inclined plane.

B.3 Impact

The impact happens at $t = t_i$, when there is contact between the disk and the plane, i.e. $c_n(t_i) = R$, which leads to

$$t_i = \sqrt{\frac{2h}{g\cos\alpha}}.$$

During the contact, we denote by P the point of the particle touching the plane. Its velocity is

$$\mathbf{v}_P = v_{P,n}\mathbf{n} + v_{P,T}\mathbf{t} \quad \text{with} \quad v_{P,n} = v_n, \quad v_{P,T} = v_T + R\omega.$$

As long as the disk touches the plane, it is subject to the contact force $\mathbf{r} = r_n\mathbf{n} + r_T\mathbf{t}$ that obeys the Coulomb's law:

$$\text{if } v^+_{P,T} \neq 0 \text{ (sliding motion)}, \quad r_T = -\mu\,|\,r_n\,|\,\frac{v^+_{P,T}}{\left|\,v^+_{P,T}\,\right|}, \tag{46}$$

$$\text{if } v^+_{P,T} = 0 \text{ (no slip)}\ , \quad |\,r_T\,| \leq \mu\,|\,r_n\,|\,, \tag{47}$$

where μ is the friction coefficient.

At impact time t_i, the velocities being discontinuous, it yields to Dirac delta reaction forces $\mathbf{r}$. If the subscript *plus* (resp. *minus*) denotes the right-sided (resp. left sided) limit of a quantity at time t_i, the equations of motions are,

$$m\left(v_T^+ - v_T^-\right) = r_T^i, \tag{48}$$

$$m\left(v_n^+ - v_n^-\right) = r_n^i, \tag{49}$$

$$J\left(\omega^+ - \omega^-\right) = Rr_T^i, \tag{50}$$

where (r_n^i, r_T^i) are the intensities of the Dirac reaction forces.

From B.2, we have that, just before the impact, at $t = t_i^-$, the velocities are given by,

$$v_T^- = v_T(t_i^-) = g\sin\alpha t_i, \tag{51}$$

$$v_n^- = v_n(t_i^-) = -g\cos\alpha t_i, \tag{52}$$

$$\omega^- = \omega(t_i^-) = 0. \tag{53}$$

Since equation (49) is not coupled with (48) and (50), we can solve the normal problem. The distance between the disk and the plane is 0 and the disk cannot overlap the plane so that $v_n^+ = 0$. Then, equation (49) yields $r_n^i = mg\cos\alpha t_i$.

The remaining of the section is dedicated to the resolution of the tangential problem (48) and (50).

1. Let us first assume there is no slip. We have $v_{P,T}^+ = v_T^+ + R\,\omega^+ = 0$. This, together with (53), (50) and the formula for J yields
$$r_T^i = -\frac{m}{3} v_T^-.$$
Then, using (48) and (50) leads to
$$\begin{aligned} v_T^+ &= \frac{2}{3} v_T^-, \\ \omega^+ &= -\frac{2}{3R} v_T^-. \end{aligned}$$
From Coulomb's law (47) we obtain a necessary condition for non-slipping motion: $\mu \geq \frac{\tan\alpha}{3}$.

2. Case 1: $\mu < \frac{\tan\alpha}{3}$.
From the above, there is a sliding motion: $v_{P,T}^+ \neq 0$.
   (a) Let us first show that $v_{P,T}^+ > 0$. If $v_{P,T}^+ < 0$, Coulomb's law leads to
   $$r_T^i = \mu |r_n^i| = -m\mu v_n^-,$$
   and from (48-50) we have
   $$\begin{aligned} v_T^+ &= v_T^- - \mu v_n^-, \\ \omega^+ &= -\frac{2\mu v_n^-}{R}. \end{aligned}$$
   Then, using (51-53), one can show that $v_{P,T}^+ = g\,(\sin\alpha + 3\mu\cos\alpha)\,t_i > 0$, which is in contradiction with the hypothesis $v_{P,T}^+ < 0$. Therefore, $v_{P,T}^+ > 0$
   (b) Since $v_{P,T}^+ > 0$, similar computations lead to,
   $$\begin{aligned} r_T^i &= \mu m v_n^-, \\ v_T^+ &= v_T^- + \mu v_n^-, \\ \omega^+ &= \frac{2\mu v_n^-}{R}. \end{aligned}$$
   Let us notice that $v_{P,T}^+ = g\cos\alpha t_i(\tan\alpha - 3\mu) > 0$.

3. Case 2: $\mu \geq \frac{\tan\alpha}{3}$.
Let us first show that, in that case, the particle undergoes a no slip motion. If it was sliding, ($v_{P,T}^+ \neq 0$) one can consider the two following cases, depending on the sign of $v_{P,T}^+$:
   (a) If $v_{P,T}^+ < 0$, the same computation as in (2a) leads to the same contradiction.
   (b) If $v_{P,T}^+ > 0$, the same computation as in (2b) gives $v_{P,T}^+ = g\cos\alpha t_i(\tan\alpha - 3\mu) < 0$, which is again in contradiction with the hypothesis.

   Therefore, $v_{P,T}^+ = 0$ and there is no slip. Then, using the results from (1) we have
   $$\begin{aligned} r_T^i &= -\frac{m}{3} v_T^-, \\ v_T^+ &= \frac{2}{3} v_T^-, \\ \omega^+ &= -\frac{2}{3R} v_T^-. \end{aligned}$$

B.4 Motion on the plane

We now consider the case $t > t_i$. After the impact, the disk moves on the plane and the equations of motion are

$$m\frac{dv_T}{dt} = mg\sin\alpha + r_T, \tag{54}$$

$$m\frac{dv_n}{dt} = -mg\cos\alpha + r_n, \tag{55}$$

$$J\frac{d\omega}{dt} = Rr_T. \tag{56}$$

The disk remains in contact with the plane, so $v_n = 0$ and (55) yields $r_n = mg\cos\alpha$. The particle do not undergo anymore impacts and the motion is smooth.

1. To solve the tangential problem (54, 56), let us first assume there is no slip. In that case, we have $v_{P,T} = v_T + R\omega = 0$ so that
$$\frac{d\omega}{dt} = -\frac{1}{R}\frac{dv_T}{dt}$$
This, together with (54) and (56) gives
$$r_T(t) = -\frac{mg\sin\alpha}{3}$$
and using again (54) and (56) yields
$$v_T(t) = \frac{2g\sin\alpha}{3}(t - t_i) + v_T^+,$$
$$\omega(t) = -\frac{2g\sin\alpha}{3R}(t - t_i) + \omega^+.$$
Then, Coulomb's law (47) gives the same necessary condition for non-slipping motion as before: $\mu \geq \frac{\tan\alpha}{3}$.

2. Case 1: $\mu < \frac{\tan\alpha}{3}$.
From the above, there is a sliding motion ($v_{P,T} \neq 0$). From B.3(2a), we have $v_{P,T}(t_i^+) > 0$. Then, as long as $v_{P,T} > 0$, following similar computations as before, we obtain
$$v_T(t) = g(\sin\alpha - \mu\cos\alpha)(t - t_i) + \left(v_T^- + \mu v_n^-\right),$$
$$\omega(t) = -\frac{2g\mu\cos\alpha}{R}(t - t_i) + \frac{2\mu}{R}v_n^-,$$
$$r_T(t) = -\mu mg\cos\alpha.$$
This leads to $v_{P,T}(t) = g\cos\alpha(\tan\alpha - 3\mu)(t - t_i) + g\cos\alpha(\tan\alpha + 3\mu)$. Then, $v_{P,T}$ is increasing and remains greater than zero so that the previous formulas are valid for any $t > t_i$.

3. Case 2: $\mu \geq \frac{\tan\alpha}{3}$.
In that case, we proved in B.3(3) that $v_{P,T}(t_i^+) = 0$. Let us first show that there is a no-slip motion for $t > t_i$. If not, there exists a time $\bar{t} > t_i$ for which $v_{P,T}(\bar{t}) \neq 0$. The motion being smooth, one can find $t^* > t_i$ and $\delta > 0$ such that $v_{P,T}$ do not vanish on $]t^*, t^* + \delta[$ and $v_{P,T}(t^*) = 0$. We then have to deal with two cases:

   (a) $v_{P,T}(t) < 0$ on $]t^*, t^* + \delta[$ for a given $\delta > 0$. Then, following the same reasoning as in the previous non-slip cases we have, for $t \in [t^*, t^* + \delta]$
   $$v_T(t) = g(\sin\alpha + \mu\cos\alpha)(t - t^*) + v_T(t^*),$$
   $$\omega(t) = \frac{2\mu g\cos\alpha}{R}(t - t^*) + \omega(t^*),$$
   $$r_T(t) = \mu mg\cos\alpha.$$
   Therefore, $v_{P,T}(t) = g(\sin\alpha + 3\mu\cos\alpha)(t - t^*) > 0,\ \forall t > t^*$, which is in contradiction with the hypothesis.

(b) Similarly, if $v_{P,T}(t) > 0$ on $]t^*, t^* + \delta[$, we have for $t \in [t^*, t^* + \delta]$

$$\begin{aligned} v_T(t) &= g(\sin\alpha - \mu\cos\alpha)(t - t^*) + v_T(t^*), \\ \omega(t) &= -\frac{2g\cos\alpha}{R}(t - t^*) + \omega(t^*), \\ r_T(t) &= -\mu mg\cos\alpha. \end{aligned}$$

Therefore, $v_{P,T}(t) = g\cos\alpha(\tan\alpha - 3\mu)(t - t_i) < 0,\ \forall t > t_i$. This is again in contradiction with the hypothesis.

So we proved that $v_{P,T}(t) = 0,\ \forall t > t_i$. Then, using computations done in (1),

$$\begin{aligned} v_T(t) &= \frac{2g\sin\alpha}{3}(t - t_i) + \frac{2}{3}v_T^-, \\ \omega(t) &= -\frac{2g\sin\alpha}{3R}(t - t_i) - \frac{2}{3R}v_T^-, \\ r_T(t) &= -\frac{mg\sin\alpha}{3}. \end{aligned}$$

References

[1] V. Acary and B. Brogliato. *Numerical Methods for Nonsmooth Dynamical Systems: Applications in Mechanics and Electronics*. Springer Science & Business Media,. 2008.

[2] V. Acary, F. Cadoux, C. Lemaréchal, and J. Malick. A formulation of the linear discrete coulomb friction problem via convex optimization. *ZAMM-Journal of Applied Mathematics and Mechanics/Zeitschrift für Angewandte Mathematik und Mechanik*, 91(2):155–175, 2011.

[3] M. Andersen, J. Dahl, Z. Liu, L. Vandenberghe, S Sra, S Nowozin, and SJ Wright. Interior-point methods for large-scale cone programming. *Optimization for machine learning*, 5583, 2011.

[4] M. Anitescu. Optimization-based simulation of nonsmooth rigid multibody dynamics. *Mathematical Programming*, 105(1):113–143, 2006.

[5] M. Anitescu and Gary D. Hart. A constraint-stabilized time-stepping approach for rigid multibody dynamics with joints, contact and friction. *International Journal for Numerical Methods in Engineering*, 60(14):2335–2371, 2004.

[6] M. Anitescu and F. A. Potra. Formulating Dynamic Multi-Rigid-Body Contact Problems with Friction as Solvable Linear Complementarity Problems. *Nonlinear Dynamics*, 14(3):231–247, 1997.

[7] M. Anitescu and A. Tasora. An iterative approach for cone complementarity problems for nonsmooth dynamics. *Computational Optimization and Applications*, 47(2):207–235, 2010.

[8] M. N. Ardekani, P. Costa, W.-P. Breugem, and L. Brandt. Numerical Study of the Sedimentation of Spheroidal Particles. *International Journal of Multiphase Flow*, 87:16–34, 2016.

[9] F. Bernicot and A. Lefebvre-Lepot. Existence results for non-smooth second order differential inclusions, convergence result for a numerical scheme and application to the modelling of inelastic collisions. *Confluentes Mathematici*, 2(4):445–471, 2010.

[10] E. Corona, D. Gorsich, P. Jayakumar, and S. Veerapaneni. Tensor train accelerated solvers for nonsmooth rigid body dynamics. *Applied Mechanics Reviews*, 71(5), 2019.

[11] E. Corral, R.G. Moreno, M.J.G. García, and C. Castejón. Nonlinear phenomena of contact in multibody systems dynamics: a review. *Nonlinear Dynamics*, 2021.

[12] P.A. Cundall and O.D.L. Strack. A discrete numerical model for granular assemblies. *Géotechnique*, 29(1):47–65, 1979. Publisher: ICE Publishing.

[13] S. De, E. Corona, P. Jayakumar, and S. Veerapaneni. Scalable solvers for cone complementarity problems in frictional multibody dynamics. In *2019 IEEE High Performance Extreme Computing Conference (HPEC)*, pages 1–7. IEEE, 2019.

[14] M. Frémond. Rigid bodies collisions,. *Physics Letters A*, 204(1):33–41, 1995.

[15] M. Frémond. *Non-Smooth Thermomechanics*. Springer Berlin Heidelberg, Berlin, Heidelberg, 2002.

[16] T. Heyn, M. Anitescu, A. Tasora, and D. Negrut. Using krylov subspace and spectral methods for solving complementarity problems in many-body contact dynamics simulation. *International Journal for Numerical Methods in Engineering*, 95(7):541–561, 2013.

[17] J-B. Hiriart-Urruty and C. Lemarechal. *Convex Analysis and Minimization Algorithms I: Fundamentals*. Grundlehren der mathematischen Wissenschaften, Convex Analysis and Minimization Algorithms. Springer-Verlag, Berlin Heidelberg, 1993.

[18] M. Jean. The non-smooth contact dynamics method. *Computer Methods in Applied Mechanics and Engineering*, 177(3):235–257, 1999.

[19] M. Jean and J. J. Moreau. Unilaterality and dry friction in the dynamics of rigid body collections. In *1st Contact Mechanics International Symposium*, pages 31–48, Lausanne, Switzerland, 1992.

[20] K. Krabbenhoft, A. V. Lyamin, J. Huang, and M. Vicente da Silva. Granular contact dynamics using mathematical programming methods. *Computers and Geotechnics*, 43:165–176, 2012.

[21] Aline Lefebvre. Numerical simulation of gluey particles. *ESAIM: Mathematical Modelling and Numerical Analysis*, 43(1):53–80, 2009.

[22] A. Lefebvre-Lepot. Scopi web page, http://www.cmap.polytechnique.fr/ lefebvre/scopi/index.html, 2022.

[23] A. Lin and S.-P. Han. On the Distance between Two Ellipsoids. *SIAM Journal on Optimization*, 13(1):298–308, 2002.

[24] X. Lin and T-T. Ng. Contact detection algorithms for three-dimensional ellipsoids in discrete element modelling. *International Journal for Numerical and Analytical Methods in Geomechanics*, 19(9):653–659, 1995.

[25] S. Luding. Introduction to discrete element methods. *European Journal of Environmental and Civil Engineering*, 12(7-8):785–826, 2008.

[26] H. Martin, A. Mangeney, A. Lefebvre-Lepot, B. Maury, and Y. Maday. An Optimization-Based Discrete Element Model for Dry Granular Flows: Application to Granular Collapse on Erodible Beds, submitted, hal-03790427. 2022.

[27] B. Maury. A time-stepping scheme for inelastic collisions. *Numerische Mathematik*, 102(4):649–679, 2006.

[28] H. Mazhar, T. Heyn, D. Negrut, and A. Tasora. Using nesterov's method to accelerate multibody dynamics with friction and contact. *ACM Transactions on Graphics (TOG)*, 34(3):1–14, 2015.

[29] D. Melanz, L. Fang, P. Jayakumar, and D. Negrut. A comparison of numerical methods for solving multibody dynamics problems with frictional contact modeled via differential variational inequalities. *Computer Methods in Applied Mechanics and Engineering*, 320:668–693, 2017.

[30] M. Monteiro Marques. *Differential Inclusions in Nonsmooth Mechanical Problems: Shocks and Dry Friction*. Birkhäuser, 2013.

[31] J.J. Moreau. Unilateral Contact and Dry Friction in Finite Freedom Dynamics. In J.J. Moreau and P.D. Panagiotopoulos, editors, *Nonsmooth Mechanics and Applications*, International Centre for Mechanical Sciences, pages 1–82. Springer, Vienna, 1988.

[32] J.J. Moreau. Numerical aspects of the sweeping process. *Computer Methods in Applied Mechanics and Engineering*, 177(3-4):329–349, 1999.

[33] MOSEK. Mosek web page, https://www.mosek.com/, 2022.

[34] Y. Nesterov. A method of solving a convex programming problem with convergence rate O (1/k2). *Sov. Math. Dokl*, 1983.

[35] E. G. Nezami, Y. M.A. Hashash, D. Zhao, and J. Ghaboussi. A fast contact detection algorithm for 3-D discrete element method. *Computers and Geotechnics*, 31(7):575–587, 2004.

[36] L. Paoli and M. Schatzman. A Numerical Scheme for Impact Problems I and II. *SIAM Journal on Numerical Analysis*, 40(2):702–733, 2002.

[37] C. Petra, B. Gavrea, M. Anitescu, and F. Potra. A computational study of the use of an optimization-based method for simulating large multibody systems. *Optimization Methods & Software*, 24(6):871–894, 2009.

[38] F. Pfeiffer and C. Glocker. *Multibody dynamics with unilateral contacts*. John Wiley & Sons, 1996.

[39] D. E. Stewart and J. C. Trinkle. An Implicit Time-Stepping Scheme for Rigid Body Dynamics with Inelastic Collisions and Coulomb Friction. *International Journal for Numerical Methods in Engineering*, 39(15):2673–2691, 1996.

[40] D.E. Stewart. Convergence of a Time-Stepping Scheme for Rigid-Body Dynamics and Resolution of Painlevé's Problem. *Archive for Rational Mechanics and Analysis*, 145(3):215–260, 1998.

[41] A. Tasora and M. Anitescu. A convex complementarity approach for simulating large granular flows. *Journal of Computational and Nonlinear Dynamics*, 5(3):1–10, 2010.

[42] A. Tasora and M. Anitescu. A matrix-free cone complementarity approach for solving large-scale, non-smooth, rigid body dynamics. *Computer Methods in Applied Mechanics and Engineering*, 2011.

[43] A Tasora, D Negrut, and M Anitescu. Large-scale parallel multi-body dynamics with frictional contact on the graphical processing unit. *Proceedings of the Institution of Mechanical Engineers, Part K: Journal of Multi-body Dynamics*, 222(4):315–326, 2008.

[44] H. Uzawa. Iterative methods for concave programming. *Studies in linear and nonlinear programming*, 6:154–165, 1958.

[45] X. Zheng, W. Iglesias, and P. Palffy-Muhoray. Distance of closest approach of two arbitrary hard ellipsoids. *Physical Review E*, 79(5):057702, 2009.